July 2021

GAS EVOLUTION PHENOMENON OF METHANE IN BASE FLUIDS OF NON-AQUEOUS DRILLING MUDS UNDER CONTROLLED DEPRESSURIZATION

Damilola Ojedeji
Louisiana State University and Agricultural and Mechanical College

GAS EVOLUTION PHENOMENON OF METHANE IN BASE FLUIDS OF NON-AQUEOUS DRILLING MUDS UNDER CONTROLLED DEPRESSURIZATION

A Thesis

Submitted to the Graduate Faculty of the
Louisiana State University and
Agricultural and Mechanical College
in partial fulfillment of the
requirements for the degree of
Master of Science

in

The Craft & Hawkins Department of Petroleum Engineering

by
Damilola Oluwafemi Ojedeji
B.S., University of Lagos, Nigeria, 2016
August 2021

To my father and mother, Oluwole and Mujidat Ojedeji, who taught me to always work hard and believe in God

To my brothers, Abiola and Bolaji Ojedeji who were always there when I needed someone to talk to.

ACKNOWLEDGMENTS

I would like to specially thank my advisor, Dr. Yuanhang Chen, for his guidance and support throughout this journey. I would also like to thank the rest of my committee members, Dr. Paulo Waltrich and Dr. Clint Aichele for their time and support during this process. I would like to say a special thank you to my research group members, Scott Perry and Shahriar Mahmud, who have been very helpful and supportive during my time at LSU. Finally, I would like to thank my parents for their exceptional support and guidance through the years. My brother, Abiola was always there through thick and thin. I will forever be grateful for his kindness and encouraging words.

TABLE OF CONTENTS

LIST OF TABLES

LIST OF FIGURES

NOMENCLATURE

Alk	Alkalinity [mg/L]
C_L	Existing concentration of gas [kmol/m^3]
$C_L^{t=t_1}$	Concentration of gas in the liquid phase at $t = t_1$
$C_L^{t=t_2}$	Concentration of gas in the liquid phase at $t = t_2$
C_o	Initial concentration [kmol/m^3]
C_s	The saturated dissolved gas molar or mass concentration in the liquid [mol/l]
d	Diameter (m)
f^g	Fugacity of gas in the gas phase[atm]
F_w	Frictional losses [lbm/s^2]
G	Gas side volumetric flow rate [m^3/s]
H	Henry's law constant [psi]
$(H.T.U.)$	Height of an over-all transfer unit based on liquid film concentrations, [ft]
j	Flux [mol/m^2/s]
k	Mass transfer coefficient [1/s]
K_La	Desorption/degassing/mass transfer coefficient [1/s]
$[K_La]$	Instantaneous Desorption Coefficient [1/s]
$[K_La]_{max}$	Maximum Instantaneous Desorption Coefficient [1/s]
K_La_b	Volumetric liquid side mass transfer coefficient from bubbles generated [1/s]
l	The current gas loading in the liquid phase which is defined by the total moles of gas per total moles of the liquid phase, dimensionless.
l_{max}	The gas loading of the fluid at saturation for a specific pressure, dimensionless.

l_0	The initial gas loading in the liquid phase when saturated at a specific starting pressure, dimensionless.
L	Liquid rate $[m^3/s]$
M	Molecular weight of gas entering column [g/gmol]
n	speed [rev/s]
N_A	Mass transfer rate [kmol/s].
P	Pressure [MPa]
P_1	Absolute Pressure in test section 1 at a particular time [Mpa].
P_t	Pressure of gas in the second test sections at a specific time [MPa]
$P_{t=0}$	Pressure in the second test section at time t = 0, usually atmospheric pressure [MPa]
R	Gas constant $[l \cdot atm \cdot K^{-1} \cdot mol^{-1}]$;
Re	Reynold's number
S_p	Pressure source term $[pa/ft]$
qi	Actual flow rate of gas desorbing from liquid [m^3/s]
q_o	Evolved gas flow rate measured by the flow meter [m^3/s]
$S_p(w)$	Source term vector
t	Time[s]
T	Liquid temperature [K]
TDS	Total dissolved solid [mg/L]
T_E	Time required for the evolution of one-half the total evolved gas [s]
T_0	Temperature condition in the flow meter, 273k
T_1	Temperature of the first test section[K] - Room temperature, 298k
U	Partial molar volume of gas in solution
$v_{g,l,m}$	Gas, liquid, mixture velocity $[ft/s]$

V	Volume of the reactor [m^3]
V_1	Total Volume of gas that comes out from solution at any time t, converted to conditions in flow meter at $T = 0℃$ and $P = 1$ atm. [m^3]
$V_I^{'}$	Total volume of gas that comes out from solution at t, at pressure condition of test section I and at room temperature [m^3]
V_{II}	Total volume of gas removed from section II [m^3]
V_B	Total volume of blanket gas in test section II as measured by the flowmeter [m^3]
$V_B^{'}$	Original total volume of blanket gas in test section II at P_1[m^3]
V_L	Liquid volume [m^3]
V_t	Volume of the first test section [m^3]
V_T	Total volume of gas that comes out of the system [m^3]
V_v	Total volume of voids in section II [m^3]
$w_{1,2}$	Conservative variables [ppg]
We	Weber number
x	Mole fraction of dissolved gas in liquid at equilibrium condition
X	lb. solute/lb. water
X^*	Equilibrium lb. solute/lb. water
Z	Column operating height [ft]

Greek Letters

$\alpha_{g,l}$	Gas, liquid hold up, dimensionless
$\Delta P/\Delta t$	Average rate of pressure drop in the first 5 seconds [MPa/s].
Δt	time step [s]
Γ_g	Mass transfer term [kg/s^2]
ρ	Density [kg/m^3]

μ	Viscosity [Pa.s]
γ	Surface tension [N/m]

Subscripts

b	Bulk
e	Equilibrium
eff	Effective
g	Gas side
i	Interface
I	Initial
l	Liquid side
m	Distribution coefficient
o	Distribution coefficient
oL	Overall
s	stirrer
t	time

SI Metric Conversion Factors

psi	× 0.006895	=	MPa
ft	× 3.048* E– 01	=	m
liters	× 1* E– 03	=	m^3

*Conversion factor is exact

ABSTRACT

As wells become more complex and drilling conditions to reach targets prove even more challenging, being able to detect influx event early and safely handle these influxes has become one of the most important focus areas for improvement in well control safety. The high solubility of formation gas in non-aqueous drilling fluids however makes kick detection and safe handling of kicks more complicated. Recent studies are beginning to incorporate desorption kinetics in well control models to simulate the transient multiphase flow phenomenon associated with gas kicks in non-aqueous drilling fluids to foster safe handling of kicks. However, there is currently an inadequate understanding of gas evolution from non-aqueous fluids to correctly integrate desorption kinetics in these models. Therefore, the aim of this thesis was to improve the understanding of gas evolution in non-aqueous fluids by developing a controlled depressurization experiment that accurately simulate desorption during well control events. Gas evolution experiments were conducted in a custom-made apparatus using methane as the gas phase with various liquid phases. Different parameters such as initial saturation pressure, depressurization rate, oil-water ratio, presence of surfactant, different base fluids, and viscosity, that could influence the behavior of gas desorbing from solutions have been investigated. All these parameters except for the presence of surfactant were found to influence gas evolution. From these studies, the time dependency of the desorption process was presented for methane in olefins. Desorption coefficient results obtained from this study are instrumental in incorporating the desorption kinetics in models to understand its impact on riser/wellbore unloading. The improved understanding of the gas evolution process will ultimately enhance the current practices of safely handling influxes in non-aqueous drilling muds.

Chapter 1. INTRODUCTION

1.1. Drilling Fluids

Drilling fluids are very crucial to the cost and successful completion of an oil well. The choice of the drilling fluid type and the maintenance of the right properties could significantly affect the duration and consequently the total cost of drilling (Caenn, Darley, & Gray, 2011). Drilling fluids serve a multitude of functions from removal of cuttings and maintaining wellbore stability to lubricating and cooling of bit, among others. They are typically classified according to their base into aqueous drilling fluids (ADFs), non-aqueous drilling fluids (NADFs) and gaseous drilling fluids. The selection of the most suitable base fluid depends on a few factors including cost, technical performance, and environmental impact. Aqueous drilling fluids are the most widely used and are considered less expensive than oil base muds. However, they are not suitable for drilling shale formations due to the interaction of water with clay minerals resulting in shale swelling. On the other hand, non-aqueous drilling fluids can support shale formation and are therefore used when well conditions call for reliable shale inhibition.

1.1.1. Non-Aqueous Drilling Fluids

Non-aqueous drilling fluids were introduced and developed to address drilling problems that aqueous based muds could not handle. They are typically formulated with diesel, mineral oil or low toxicity linear olefins and paraffin, which are sometimes referred to as synthetics. NADFs offer several advantages over aqueous drilling fluids; including stabilization of formation clays, high temperature tolerance, lubricity, corrosion control, etc.(Boesch & Rabalais, 1987; Caenn et al., 2011; Growcock & Patel, 2011). However, non-aqueous based muds pose significant challenges such as high initial cost, inability to detect gas kicks etc.

1.2. Challenges with the use of non-aqueous drilling fluids.

One of the most critical drawbacks of using non-aqueous drilling fluids (NADF) is the high capacity of these fluids to dissolve formation gas, which makes kick detection and safe handling of kicks more complicated than in aqueous drilling fluids(O'Bryan, 1985). Therefore, the release of formation gas from NADFs as they are circulated out of the hole is delayed (Growcock & Patel, 2011). Gas kick indicators typically involves increased circulation rate, decreased mud weight, variation in pump pressure etc. (Grace, 2017). These indicators are easily observed when ADFs are in use. As a result, steps can be quickly taken to handle these influxes. However, with non-aqueous drilling fluids, there is a delay in the recognition of these symptoms due to gas dissolving in NADFs, thus increasing the risk of a blowout. With wells becoming more complex and drilling conditions to reach targets prove even more challenging, being able to detect influx event early and safely handle these influxes has become one of the most important focus areas for improvement in well control safety(Fraser, Lindley, Moore, & Vander Staak, 2014). Even with the advent of new technologies such as managed pressure drilling (MPD), early kick detection is still challenging with NADFs. Formation gas can become infinitely soluble in OBM/SBM when drilling in high pressure-high temperature wells (Gomes et al., 2018; Torsvik, Skogestad, & Linga, 2017). Therefore, gas may not desorb out of the liquid phase until the mixture migrates close to the surface, where the hydrostatic pressure above gas cut mud falls below the bubble point of the gas/drilling fluid mixture. Ultimately, this gives the drilling crew little to no time to safely handle the explosive unloading of the wellbore or riser.

1.3. Current understanding of gas kick simulation in NADFs

Different methods have been used to accurately incorporate the effects of gas solubility on kick behavior and kick handling, which would allow for better response to kick event. From purely

petroleum engineering perspective, two types of pipe-flow models have been used (Z. Ma et al., 2016): Empirical correlation models and Mechanistic models. Empirical correlations are obtained from field/experiments and therefore can be useful in certain applications. However, they are limited by fluid types, pressure, temperature, velocity ranges and certain other environmental variables (Z. Ma et al., 2016). Hence, it was imperative to develop a more physics-based approach that is peculiar to certain conditions or variables. The mechanistic approach uses fundamental equations based on mass, momentum, and energy balance equations. The most used mechanistic model is the drift flux model (DFM)(de Carvalho et al., 2019). The DFM has been used frequently in multiphase flow modeling for drilling applications. (Avelar, Ribeiro, & Sepehrnoori, 2009; Blázquez, Dalmazzone, Emond, & Schneider, 2016; Z Ma et al., 2017; Nickens, 1987; Podio & Yang, 1986; Wang, Xu, Chen, Jiang, & Liu, 2019).

The drift flux model uses a combination of mass conservation and momentum equations. The governing equations of the drift flux model are two mass conservation equations and one momentum conservation equation. The system of differential equations in the drift-flux model (Eqn. 1.1-1.6) can be written in a vector form(Evje & Fjelde, 2002) generally expressed as:

$$\frac{\partial \mathrm{w}}{\partial \mathrm{t}} + \frac{\partial \mathrm{F(w)}}{\partial \mathrm{x}} = \mathrm{S_p(w)} \tag{1.1}$$

Where

$$\mathrm{w} = \begin{bmatrix} \alpha_l \rho_l \\ \alpha_g \rho_g \\ \alpha_l \rho_l v_l + \alpha_g \rho_g v_g \end{bmatrix} \tag{1.2}$$

$$\mathrm{F(w)} = \begin{bmatrix} \alpha_l \rho_l v_l \\ \alpha_g \rho_g v_g \\ \alpha_l \rho_l v_l^2 + \alpha_g \rho_g v_g^2 + \mathrm{p} \end{bmatrix} \tag{1.3}$$

$$\mathrm{S_p(w)} = \begin{bmatrix} \Gamma_g \\ -\Gamma_g \\ -S_p \end{bmatrix} \tag{1.4}$$

The system can then be expressed in the form:

$$\partial_t \begin{bmatrix} w_1 \\ w_2 \\ w_3 \end{bmatrix} + \partial_x \begin{bmatrix} v_l w_1 \\ v_g w_2 \\ v_l^2 w_1 + v_g^2 w_2 + p(w_1, w_2) \end{bmatrix} = \begin{bmatrix} \Gamma_g \\ -\Gamma_g \\ -S_p \end{bmatrix} \tag{1.5}$$

Where

$$\Gamma_g = \alpha_l \rho_l \frac{\partial l}{\partial t} \tag{1.6}$$

$$\frac{\partial l}{\partial t} = f(K_L a) \tag{1.7}$$

Where l is the existing gas loading in the liquid phase which is defined by the total moles of gas per total moles of the liquid phase and needs to be predicted from experiments based on a desorption kinetics model as shown in Eqn. 1.7. One of the most common assumptions in the use of this model is that the absorption and desorption of the gas phase in non-aqueous fluid (NAF) is instantaneous (Z Ma et al., 2018), which does not accurately predict the hydrodynamics of gas influxes in the well. Multiple studies have therefore shown that gas desorption is indeed time dependent.(Hamborg, Kersten, & Versteeg, 2010; Huerta et al., 1996; Kierzkowska-Pawlak & Chacuk, 2010; Miranda et al., 2019; Sheng, Maini, Hayes, & Tortike, 1999). Some recent studies incorporated the consideration of desorption kinetics in well control simulations using the drift flux model.(Nwaka & Chen, 2019; Nwaka, Wei, Ambrus, & Chen, 2020; Skogestad et al., 2019). Nnamdi et al (2020)(Nwaka et al., 2020) developed a model for riser gas events with consideration of time-dependent desorption. In their work, they discussed the impact of gas desorption process on riser gas unloading and carried out sensitivity analyses on the effect of the desorption coefficient on certain variables such as gas void fraction, pressure on the Subsea Blowout preventor (SSBOP) as shown in Figure 1.1a and 1.1b.

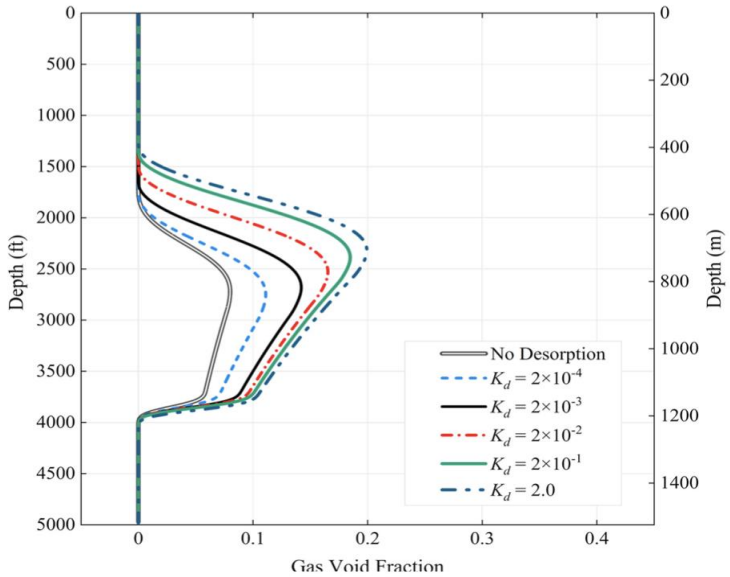

(a)

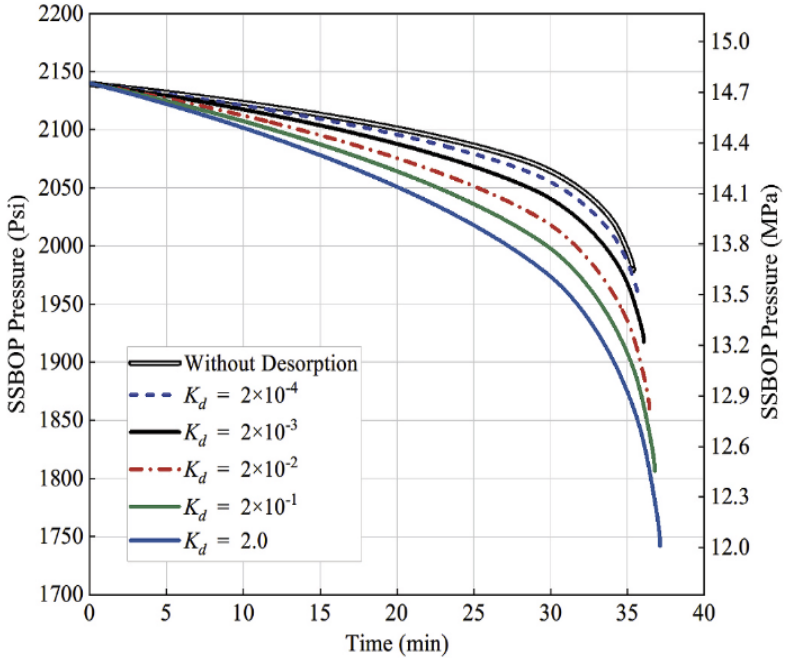

(b)

Figure 1.1. (a) Profiles of gas void fraction distribution in the riser at 20 min with different values of desorption coefficient, K_d. (b) Profiles of gas void fraction distribution in the riser at 40 min with different values of desorption coefficient, K_d (Nwaka et al., 2020)

1.4. Problem Statements and Objectives

From Figures 1a and 1b, it is evident that the desorption coefficient, shown as K_d in the figures, is an important parameter in understanding the impact of the gas evolution process on riser/wellbore unloading. However, quantify desorption coefficients that could be applied in models has being difficult at best due to the lack of comprehensive predictive models, inadequate methodologies to simulate the desorption process in a wellbore or riser, and the high dependency of the gas evolution process on the geometry of the apparatus. Therefore, the primary goal of this study is to utilize a methodology that accurately simulates the gas evolution process in a drilling scenario to better understand the time dependent mass transfer process, and ultimately improve the current practices of safe handling of influxes. Different parameters that could affect the desorption process will be thoroughly investigated and analyzed to obtain coefficients that characterizes a typical gas evolution in a drilling well/riser.

1.5. Thesis Organization.

The first chapter in this thesis provides the motivation behind the study of gas evolution as it relates to influx management. Chapter 2 gives insights into the different methodologies that have been used to study gas evolution and the models that have been applied to characterize the process. Chapter 3 goes over the experimental development, while chapter 4 presents the materials used and the experimental design. The results obtained for the investigated parameters are presented in Chapter 5. Chapter 6 provides the major conclusions from this investigation and chapter 7 contains the recommendations for future work.

CHAPTER 2. GAS-LIQUID MASS TRANSFER

Gas-liquid mass transfer in non-reactive systems is a common phenomenon observed in various industrial applications. For instance, in wastewater treatment application, desorption of CO_2 is performed to remove organic and calcium from wastewater (Y. Kim, Han, & Lee, 2003; Y. H. Kim, Yeom, Ryu, & Song, 2004; Lisitsin, Hasson, & Semiat, 2008). In refrigeration, to understand foaming properties of refrigerant/lubricant mixture, refrigerant desorption has been studied (Becerra & Parise, 2003; Fortkamp & Barbosa Jr, 2015; Goswami et al., 1997). It is also present in the oil industry; especially in separators where desorption is taken into consideration while designing compact separators (Lavenson et al., 2016). The performance of solution gas drive in heavy oil reservoirs are also impacted by the kinetics of desorption of dissolved gas(Pooladi-Darvish & Firoozabadi, 1999; Sheng et al., 1999). In this study, however, gas evolution is studied with the aim of tackling issues relating to safe handling of kicks when formation gas dissolves in non-aqueous drilling fluids

2.1 Solubility

Solubility has been shown to play an important role in understanding the behavior of gas kicks in non-aqueous drilling fluids (Gu et al., 2021; Manikonda, 2020; Swanson, Gilvary, & McEwan, 1988; Xu, Song, Li, Zhu, & Zhu, 2019). The solubility of gas is commonly calculated using the simple Henry's law which is given by Eqn. 2.1.

$$\mathrm{P} = \mathrm{Hx} \tag{2.1}$$

Where $P =$ gas pressure [psi]; $H =$ Henry's law constant [psi]; $x =$ mole fraction of dissolved gas in liquid at equilibrium condition. At a given pressure, Henry's law can be applied to determine the amount of gas that dissolves in solution, which is in turn used to obtain the initial gas

concentration in the liquid phase when saturated at a specific pressure, and the saturated dissolved gas molar or mass concentration in the liquid, C_s.

However, Henry's law as given in Eqn. 2.1 above only applies to an ideal gas or low-pressure conditions (Xu et al., 2019). It has been discovered that if the pressure is sufficiently high (> 20 atm) as seen in the case of deep-water drilling, Eqn. 2.1 is found to break down (King, 2013; Lekvam & Bishnoi, 1997; Weiss, 1974). King (1969) presented a modified form of Henry's law for the solubility of slightly soluble gases at elevated pressures as shown in Eqn. 2.2.

$$f^g = H \cdot \exp\left(\frac{10^6 PU}{RT}\right) \tag{2.2}$$

Where f^g =fugacity of gas in the gas phase[atm]; U = partial molar volume of gas in solution [l/mol]; R = Gas constant, $0.08205[l \cdot atm \cdot K^{-1} \cdot mol^{-1}]$; T = liquid temperature [K]

Eqn. (2.2) reduces to Eq. (2.1) as $P \rightarrow 0$

Eqn. 2.2 can be applied to accurately determine the amount of gas that dissolves in a solution at high pressure. The partial molar volume obtained from Eqn. 2.2 is converted to concentration of gas in the liquid phase.

2.2 Bubble Dynamics

To describe the physics of riser gas in a NAF system, it is imperative to understand the so-called "Evolution cycle of a bubble". This cycle predominantly follows four stages namely: bubble nucleation, growth, rise, and coalescence. The nucleation of the bubble is mainly driven by the degree of super saturation of the bulk fluid (Lavenson et al., 2016). Jones et.al. reported four different types of nucleation that could occur in a supersaturated liquid(Jones, Evans, & Galvin, 1999). Type 1 and type 2 are known as homogeneous and heterogeneous nucleation. These two types of nucleation (also known as classical nucleation) require the super saturation ratio to be in

the order of 100 or even more (Hemmingsen, 1975). Type 3 nucleation; also known as pseudo-classical nucleation; occurs at pre-existing gas cavities(Alden Brack Daniel, 2018). Type 4 nucleation occurs if cavities exist where the radii of curvature are greater than the critical bubble radius. During the experimental investigation done for the current work, the super saturation ratio was significantly low to make the case for classical nucleation. Hence, types 1 and 2 are not thought to be relevant for this work. After the bubble is formed, its growth depends on certain parameters such as the diffusion rate, liquid inertia, viscosity, gas superficial velocity, and surface tension (de Carvalho et al., 2019; Lavenson et al., 2016). The dynamics of bubble rise are also influenced by parameters such as buoyancy, drag, viscosity, surface tension, and gravity. Bubbles, while rising, may coalesce as it grows bigger and bigger due to hydrostatic pressure reduction. However, within the range of the experimental setup height used for this work, bubble coalescence was not observed, so will not be discussed further.

2.3. Previous Mass transfer Experimental Designs

Desorption mass transfer coefficient is a crucial parameter in understanding the rate of gas evolution from non-aqueous based fluids. While it is evident that gas evolution depends on multiple parameters as mentioned in the previous section, the effect of each of these parameters, except for concentration difference, is reflected in the value of the mass transfer coefficient. Various methods have been utilized by different studies to investigate the effect of some of these parameters on the mass transfer behavior of fluid systems. The basis of these desorption experiments was to create an approach for the evolution of gas from liquid. The approach may include stripping, agitation by stirring, depressurization or any combination thereof.

2.3.1. Desorption based on stirring, stripping and depressurization

One of the most common ways desorption has been investigated involved the combination of stirring, stripping and depressurization. Welland et al investigated the desorption of CO_2 from water in a stirred Pyrex vessel(Weiland, Thuy, & Liveris, 1977). The experiment involved absorption followed by desorption initiated by a combination of stirring, stripping and depressurization. Water was first introduced into the stirred vessel and was thoroughly flushed by carbon dioxide until the water is saturated. Once the system had approximately equilibrated, the cell pressure was slowly reduced to prevent massive bubbling and concomitant loss of dissolved gas. The stripping gas was then introduced into the vessel and the stirrer was turned on. The exit gas samples were collected every 15 seconds to obtain the data required to compute the mass transfer coefficient. Two types of desorption phenomena were observed: bubble desorption and quiescent desorption. Bubble desorption occurs when the level of saturation was high and therefore had a high mass transfer coefficient, and quiescent desorption, with a low K_La value occurs at a moderate to low saturation level. This conclusion was in agreement with the ones made by Thuy et al and Hikita & Konish for CO_2 desorbing from water using similar methodology (Hikita & Konishi, 1984; Thuy & Weiland, 1976). Hikita and Konishi further found K_La to be proportional to the liquid stirring speed, diameter of the liquid stirrer and temperature. Al hindi et al(Al-Hindi & Azizi, 2018) conducted similar desorption experiments of CO_2 from different water types in a mechanically agitated tank. They concluded that the mass transfer coefficient increases with both gas flow rate and stirring speed but decreases with increase in salinity until a certain critical value was reached beyond which mass transfer increased again. Panja & Roa, and Lisitsin et al(Lisitsin et al., 2008; Panja & Phaneswararao, 1994) also used identical set up to investigate desorption of

carbon dioxide from water. They reported that K_La increases with both stripping gas flow rate and stirring speed.

2.3.2. Desorption based on stripping and depressurization

A few others carried out desorption experiments with stripping and depressurization as the major way of initiating gas evolution. Shulman & Molstad (Shulman & Molstad, 1950) investigated the desorption of CO_2 from water in a bubble column. In their experiment, the solute (carbon dioxide) was first dissolved in water in a column packed with rasching tings. The saturated water then enters a bubble column. Air which is used as stripping gas is then fed into the liquid through the bottom of the column as bubbles. Samples of water entering and leaving the column were then collected for measurements. From their investigations, they concluded that the mass transfer coefficient is a function of liquid rate, water temperature, column height and liquid diffusivity. Other investigators used a similar method of desorption initiation to study the effect of temperature on mass transfer coefficient of Carbon dioxide from tap water in counter current packed tower, using air as stripping gas (Rixon, 1948; Sherwood, Draemel, & Ruckman, 1937; Sherwood & Holloway, 1940). The authors concluded that an increase in temperature led to an increase in desorption coefficient. Sherwood et al (1937), Sherwood and Holloway (1940), Rixon (1948) and Voyer & Miller (1968) (Rixon, 1948; Sherwood et al., 1937; Sherwood & Holloway, 1940; Voyer & Miller, 1968) all reported that volumetric mass transfer coefficient is independent of flowrate of stripping gas but increases with increase in Liquid flow rate.

2.3.3. Desorption based on stirring and depressurization – Gas evolution in a closed system

Few studies carried out desorption experiments by initiating gas evolution by depressurization followed by stirring. Also, this methodology involves observing the pressure build up in a closed system as gas evolution occurs. Kierzkowska-Pawla and Chacuk(Kierzkowska-Pawlak & Chacuk,

2010) studied the desorption of gas from a supersaturated solution. They used a stirred reactor vessel equipped with an impeller to obtain desorption coefficients of carbon dioxide from saturated organic solvents. The experiment consisted of two steps, absorption and subsequent desorption initialized by a pressure release. The system was depressurized via a release valve to impose the required super saturation of the solution, which led CO_2 to be released from the liquid. The corresponding pressure increase was then recorded up to another gas-liquid equilibrium pressure. The authors concluded that an increase in temperature and stirring speed enhances the desorption rate of gas from liquid. Schweitzer and Szebehely (Szebehely, 1951) previously used similar methodology to examine the desorption of air from liquids of different kinematic viscosities. The authors were able to show that desorption rate reduces with kinematic viscosity of the liquid phase.

However, most of the investigations discussed so far have used carbon dioxide/air as the gas phase. Only few authors have studied desorption of gas using a different gas phase other than CO_2 or air. Daniel et al(Alden B Daniel, Mohammad, Miranda, & Aichele, 2019) investigated the effect of initial saturation pressure and mixing speed on the mass transfer coefficient of methane from n-dodecane liquid. They concluded that changing the initial saturation pressure had a minimal effect on mass transfer coefficient but increasing the mixing speed led to an increase in the mass transfer coefficient. Miranda et al(Miranda et al., 2019) did a follow up study on the influence of surfactant and water droplet size on the volumetric mass transfer coefficient. They concluded that the effect of surfactant on mass transfer coefficient is negligible at the investigated surfactant concentration. Also, they showed that smaller water droplet sizes resulted in smaller mass transfer coefficients.

2.3.4. Desorption based on depressurization only – Gas evolution in an open system.

The studies discussed above give insights into the different methods used for investigating mass transfer and the different parameters that could affect mass transfer coefficient. The

desorption process simulated in these investigations were initiated by introducing some energy into the system in the form of stripping or/and stirring. This does not represent the desorption phenomenon that may occur in a well/riser during well control scenarios. Also, as opposed to the gas evolution methodology discussed in the preceding section, the evolved gas is allowed to leave the system as gas evolution occurs for this methodology. Hence, depressurization and gas evolution occur concurrently. Grimstad et al (Grimstad, Linga, Haave, & Saasen, 2017) simulated a gas evolution methodology that could occur in a real drilling scenario. In their experiment, an initially saturated liquid at the desired pressure is depressurized by gradually lowering the control pressure of the back pressure valve to mimic the gradual reduction in pressure felt by a drilling fluid as it is circulated out of a well. Using this methodology, they were able to investigate the effect of temperature, pressure reduction rate, drill string rotational speed and base oil type on the degassing mass rate. Gas evolution has also been studied by initiating desorption with a rapid depressurization of the saturated liquid. Fortkamp et al (2014) investigated the desorption process that occurs after a sudden depressurization of a refrigerant-oil mixture. They evaluated the effect of system's temperature and overall initial refrigerant mass fraction on the foam height and refrigerant gas mass flux. In our earlier work(Ojedeji, Perry, Nielsen, & Chen), we also simulated desorption initiated solely by rapid depressurization to investigate the effect of initial saturation pressure and base oil type on mass transfer coefficient in a custom mass transfer apparatus with methane as the gas phase. A summary of selected desorption investigations, the gas liquid system studied, and the parameters examined by these studies are shown in Table 2.1

Table 2.1. Different mechanisms of desorption, gas-liquid systems, parameters studied, and the range of desorption coefficient values obtained

Mode of desorption initiation	Authors	Gas-liquid system	Parameters investigated	K_La values
Stirring, stripping, & depressurization	Thuy et al (1976)(Thuy & Weiland, 1976)	CO_2-Water	Transition from bubble to quiescent desorption	0.0005-0.015 (1/s)
	Welland et al (1977) (Weiland et al., 1977)		Transition from bubble to quiescent desorption, Desorption, compared with absorption, degree of mixing	1-40 (cm/s)
	Hikita & konishi (1984)(Hikita & Konishi, 1984)		Liquid stirrer speed, diameter of stirrer, temperature	0.06-0.3 (1/s)
	Panja & Roa (1994)(Panja & Phaneswararao, 1994)		Stripping gas flowrate, stirring speed	0.0078-0.12 (1/s)
	Panja & Roa (1994)(Panja & Phaneswararao, 1994)		Stripping gas flowrate, stirring speed	0.0078-0.12 (1/s)
	Lisitsin et al (2008) (Lisitsin et al., 2008)		Agitation speed, gas flow rate	0.01-0.033 (1/s)
	Al hindi & Azizi (2018)(Al-Hindi & Azizi, 2018)		Stripping gas flow rate, salinity and alkalinity of water, impeller speed	0.0033-0.0279 (1/s)
Stripping & depressurization	Sherwood et al (1937)(Sherwood et al., 1937)	CO_2-Water	Gas velocity, liquid temperature, liquid rate	0.0018-0.0206 (1/s)
	Sherwood and Holloway (1940)(Sherwood & Holloway, 1940)		Gas velocity, liquid temperature, liquid rate	0.0031-0.0583 (1/s)
	Rixon (1948)(Rixon, 1948)		Gas rate, liquid rate	0.0043-0.0274 (1/s)

(table cont'd.)

Mode of desorption initiation	Authors	Gas-liquid system	Parameters investigated	K_La values
Stirring, stripping, & depressurization	Panja & Roa (1994)(Panja & Phaneswararao, 1994)	CO_2-Water	Stripping gas flowrate, stirring speed	0.0078-0.12 (1/s)
	Lisitsin et al (2008) (Lisitsin et al., 2008)		Agitation speed, gas flow rate	0.01-0.033 (1/s)
	Al hindi & Azizi (2018)(Al-Hindi & Azizi, 2018)		Stripping gas flow rate, salinity and alkalinity of water, impeller speed	0.0033-0.0279 (1/s)
Stripping & depressurization	Sherwood et al (1937)(Sherwood et al., 1937)	CO_2-Water	Gas velocity, liquid temperature, liquid rate	0.0018-0.0206 (1/s)
	Sherwood and Holloway (1940)(Sherwood & Holloway, 1940)		Gas velocity, liquid temperature, liquid rate	0.0031-0.0583 (1/s)
	Rixon (1948)(Rixon, 1948)		Gas rate, liquid rate	0.0043-0.0274 (1/s)
	Shulman & Molstad (1950)(Shulman & Molstad, 1950)		Gas rate, liquid rate, water temperature, column diameter, column height. plate porosity, liquid diffusivity, desorption, compared with absorption	0.0092-0.101 (1/s)
	Voyer & Miller (1968) (Voyer & Miller, 1968)		Gas velocity, liquid velocity, column height, presence of packing	0.04-0.14 (1/s)
Stirring & depressurization-gas evolution in a closed system	Schweitzer and Szebehely (1951) (Szebehely, 1951)	Air-heavy & light lubricating oil/ aircraft engine fuel, diesel/distilled water	Kinematic viscosity	0.0135-5.415 (1/s)
	Jeelani et al (1990) (Jeelani, Fidi, & Hartland, 1990)	CO_2/marlophene-89 in water solution	Initial Absorption pressure	Foam height [15-61mm]

(table cont'd.)

Mode of desorption initiation		authors	Gas-liquid system	Parameters investigated	K_La values
Stirring & depressurization-gas evolution in a closed system		Kierzkowska-Pawla & Chacuk(2010)(Kierzkowska-Pawlak & Chacuk, 2010)	CO_2-PC/DMEPEG/NMP	Temperature, stirring speed	0.000157-0.129 (1/s)
		Hamborg et al (2010)(Hamborg et al., 2010)	Carbon dioxide-water, oxygen-water, Nitrous oxide-MDEA	Temperature, stirrer speed	k_l 3.11×10^{-6} - 2.02×10^{-5} (m/s)]
		Daniel et al (2019) (Alden B Daniel et al., 2019)	Methane-dodecane	Initial saturation pressure, mixing speed	k_l [0.000166-0.0000785] (m/s)
		Miranda et al(2019) (Miranda et al., 2019)	Methane-Tech 80/Tech80/water emulsion	Water droplet size, presence of surfactant	0.00007-0.00025 (1/s)
		Miranda et al (2020) (Miranda, Subramani, Mohammad, & Aichele, 2020)	Methane-Exssol D-110/crude oil	Temperature, Initial saturation pressure, viscosity	2×10^{-4}-1.4×10^{-3}(1/s)
		Miranda el al (2020)(Miranda, Subramani, & Aichele, 2020)	Methane-Exssol D-110	Super saturation ratio, mixing speed	$3\times 10^{-4}\times 10^{-3}$(1/s)
Depressurization only – gas evolution in an open system	Gradual Depressu-rization	Simoneau (1981)(Simoneau, 1981)	Nitrogen-water	Concentration of dissolved gas, depressurization rate	Bubble diameter [0.1-3mm]
		Grimstad et al (2017)(Grimstad et al., 2017)	Methane-normal mineral oil/linear paraffin oil	Temperature, pressure reduction rate, and base oil type	Gas release rate [0-10 l/min]
	Rapid depressur-ization	Fortkamp et al. (2014)(Fortkamp & Barbosa Jr, 2015)	R-134a/POE ISO VG 10 and R-1234yf/POE ISO VG 10	Temperature, mass concentration	Foam height [0.2-6.5 cm]
		Ojedeji et al (2020) (Ojedeji, Perry, Nielsen, & Chen, 2020)	Methane-diesel/internal olefin	Initial saturation pressure, base oil type	0.5-1.5 (1/s)
		Ojedeji & Chen (2020) (Ojedeji & Chen, 2020)	Methane-internal olefin	Viscosifier concentration	0.3-0.8 (1/s)

Numerous studies have utilized different methods to investigate gas evolution. The methodology followed by each investigator depended on the application targeted by the study. For example, removal of impurities from water usually involves the use of a different gas phase to strip out impurities, and therefore, the methodology followed for such application had to include stripping. This current study is directed at investigating gas evolution to better understand the implication of desorption kinetics on kick detection and safe handling of kicks during drilling. Consequently, desorption initiated solely by gradual depressurization, which simulates most accurately the desorption that could occur in a drilling scenario, was followed in this study.

2.4. Gas Desorption Models

2.4.1. Base model

Few models have been used to describe the transfer of a substance from the surface of another. The most used model is given by Eqn. 2.3. This equation has been used by several studies to describe the mass transfer process of gas desorbing from liquids. (Barrut, Blancheton, Champagne, & Grasmick, 2012; Alden B Daniel et al., 2019; Eshchar, Mozes, & Fediuk, 2003; Lisitsin et al., 2008; Miranda et al., 2019). In this model, the rate of gas transfer from a liquid phase is taken to be proportional to the difference between saturation concentration (C_s) and the existing concentration of gas (C_L). (Lewis & Whitman, 1924)

$$\frac{dC_{gas}}{dt} = K_L a(C_s - C_L) \tag{2.3}$$

Where $K_L a$ is the volumetric mass transfer coefficient. Integrating Eqn. 2.3, and applying initial condition of C_L (t = 0) = C_o yields Eqn. 2.4

$$\ln\left(\frac{C_s - C_o}{C_s - C_L}\right) = K_L a * t \tag{2.4}$$

2.4.1.1. Modifications of base model & applications.

Various modifications have been made to the base model presented in Eqn. 2.4. Colt et al(Colt, Watten, & Pfeiffer, 2012) presented other methods of applying Eqn. 2.4; one parameter linear regression method and two point method.

i. **One parameter linear regression method:** This method was used in ASCE (1992) and it was based on a one parameter regression of Eqn. 2.4 as given in Eqn. 2.5.

$$\ln(C_s - C_L^t) = \ln(C_s - C_o) - K_L a\,(t - t_o) \tag{2.5}$$

ii. **Two point method**: This uses only two points on the stripping curve and it was used by Boyd(Boyd, 1986). It is given in Eqn. 2.6

$$K_L a = \frac{\ln\left(C_s - C_L^{t=t_1}\right) - \ln\left(C_s - C_L^{t=t_2}\right)}{t_2 - t_1} \tag{2.6}$$

Where $C_L^{t=t_1}$= Concentration of gas in the liquid phase at $t = t_1$ and $C_L^{t=t_2}$ = Concentration of gas in the liquid phase at $t = t_2$

Hamborg et al(Hamborg et al., 2010) also presented a modification of Eqn. 2.4. by integrating a modified version of Eqn. 2.3 to model the desorption process in non-reactive systems as presented in Eqn. 2.7

$$\ln\left(\frac{C_g^b - C_g^\infty}{C_g^0 - C_g^\infty}\right) = -\frac{mV_L + V_g}{V_g V_L} K_L a * t \tag{2.7}$$

Where $m = \frac{c_l^i}{c_g^i}$

The superscripts b and i refer to bulk and interface, superscripts o and m can be regarded as a distribution coefficient, V is the volume of the reactor, V_L is the volume of the liquid phase and C refers to concentration.

Lastly, Bjørkevoll et al (Bjørkevoll, Skogestad, Frøyen, & Linga, 2018) presented a model (Eqn. 2.8) similar to Eqn. 2.3 for describing desorption kinetics of formation gas from the liquid phase. Here, gas loading, l was used instead of concentration in Eqn. 2.4.

$$\frac{dl}{dt} = k_D(l_{max} - l) \qquad l \geq l_{max} \tag{2.8}$$

Where l is the current gas loading in the liquid phase which is defined by the total moles of gas per total moles of the liquid phase, l_{max} is the gas loading of the fluid in equilibrium with a specific ending pressure and l_0 is the initial gas loading in the liquid phase when saturated at a specific pressure.

2.4.2. Other Models

Tunnat et al, (2014)(Tunnat, Behr, & Görner, 2014) used the two-film theory to examine the desorption of CO_2 from water and aqueous amine solutions using a two-film theory as given in Eqn. 2.9.

$$j = \frac{1}{\frac{1}{k_g} + \frac{RT}{H}\cdot\frac{1}{k_L}}\cdot\left[\frac{P_{CO_2}}{H} - C_b\right] \tag{2.9}$$

Where j = flux ($mol/m^2/s$) k_g = gas side mass transfer coefficient (1/s), k_L = Liquid side mass transfer coefficient (1/s) R = gas constant, T = temperature (k), P_{CO_2} = partial pressure of CO_2, H

Henry coefficient, C_b = Concentration of component b in the liquid phase. From their investigation, they discovered that the simple two-film model represents accurately the desorption process of carbon dioxide from a simple physical solvent such as water. However, for CO_2 in aqueous amine solutions, the resulting flux is significantly higher than previously published results for CO_2 loading higher than 0.5.

Other models used by investigators and some of the correlations that were developed are shown in Table 2.2. The correlations shown here were developed based on a methodology different from the methodology that was followed in this study. Some of these models are tested with our experimental data and a model that best represents the desorption data will be used to analyze the results in this thesis

Table 2.2. Desorption models used and correlations developed

Authors	Mode of Desorption	Base Model used	K_La Correlation developed
Sherwood et al (1937)	Stripping and depressurization	$\frac{\text{Volume of } CO_2 \text{absorbed}}{\text{time taken}}$ assumed absorption = desorption	$K_La = 0.021L^{0.88}$
Shulman & Molstad (1950)	Stirring and depressurization	$K_La = \frac{L}{H.T.U._{oL} \cdot \rho}$ $H.T.U._{oL} = \frac{Z}{\int_{X_1}^{X_0} \frac{dX}{(X - X^*)}}$	Streamline region $(H.T.U.)_L = (1.35 \times 10^{-5}) \frac{(L+10730)}{l^{0.38}} \left(\frac{M}{G}\right)^{0.74} (Z)^{0.36} (\frac{\mu}{\rho D})^{0.33}$ Turbulent region: $(H.T.U.)_L = (4.0 \times 10^{-8})(L + 5530)(t)^{0.48}(Z)^{0.36}(\frac{\mu}{\rho D})^{1.86}$
Weiland et al (1977)	Stirring, stripping and depressurization	$K_La = \frac{R}{V}(C_L - C_s)$	-
Kierzkowska-Pawla and Chacuk (2009)	Stirring and depressurization	$N_{A,des} = (K_La)_{des} V_L (C_{AL} - C^*_{AL})$ $N_{A,abs} = (K_La) V_L (C^*_{AL} - C_{AL})$	$\frac{K_L a_b}{n_s} = BRe^a We^b \sigma^c$

		$(K_L a)_{des} = K_L a + K_L a_b$	
Barrut et al (2012)	Stripping	$\frac{dC_{gas}}{dt} = K_L a(C_s - C_L)$	$(0.9 - 62D_b)G$
Al-hindi & Azizi (2018)	Stirring, stripping and depressurization	$\frac{dC_{gas}}{dt} = K_L a(C_s - C_L)$	$K_L a = 1.248 \times 10^{-5} \cdot N^{1.022} \cdot TDS^{0.011} \cdot Alk^{-0.089} \cdot G^{0.498}$

$B = 1.22 \times 10^{-6}$ $a = 0.69$ $b = 0.42$ $c = 2.2$ $Re = \frac{n_s d_s^2 \rho_L}{\mu_L}$ $We = \frac{n_s^2 d_s^3 \rho_L}{\gamma_L}$

L = Liquid rate G = gas side volumetric flow rate (m^3/s) Re = Reynolds no; We = Weber no n_s = stirring speed (rev/s) d_s = stirrer diameter (m) ρ_L = liquid density(kg/m^3), μ_L = viscosity (Pa.s) γ_L = surface tension (N/m) M = Molecular weight of gas entering column

2.5. Summary

Mass transfer of gas from a liquid surface has been previously investigated using different methods. A methodology that applies gradual depressurization of the saturated liquid phase will be used to investigate gas desorption in this study as it illustrates the desorption phenomenon that could occur during a well control scenario. Different models that have been used to characterize the desorption process were also presented in this chapter. The utilization of some of these models with our experimental data were described in chapter 5. The model that best represents the experimental data was eventually used to describe the gas evolution phenomenon.

CHAPTER 3. EXPERIMENTAL DEVELOPMENT

One of the objectives of this paper was to develop a methodology that best simulates the gas evolution phenomenon that could occur in a drilling/riser column. Previous experimental studies as discussed in Chapter 2 does not adequately simulate the gas desorption in a drilling/riser column; therefore, the applicability of their results in models that consider desorption kinetics is questionable. In this chapter, the custom-made experimental apparatus and the various methodologies that have been tested with our experimental apparatus is discussed.

3.1. Mass Transfer Experimental Apparatus

The gas evolution experiments were preformed using the custom-made mass transfer apparatus whose P&ID diagram is shown in Fig 3.1. It is made up of five different test sections that are each separated by a ball valve with each test section manufactured from a translucent PVC pipes for easier visualization of the mass transfer process. The PVC pipe has an internal and external diameter of 1in and1.25 in respectively. A vacuum pump is connected to the top of the column to help siphon fluid into the system. A pressure gauge is connected to the pressure transducer at the bottom of the test section which transmits electrical signal to the Data Acquisition System. Also, the flow rate and totalized volume is recorded with the data acquisition system connected to the flow meter.

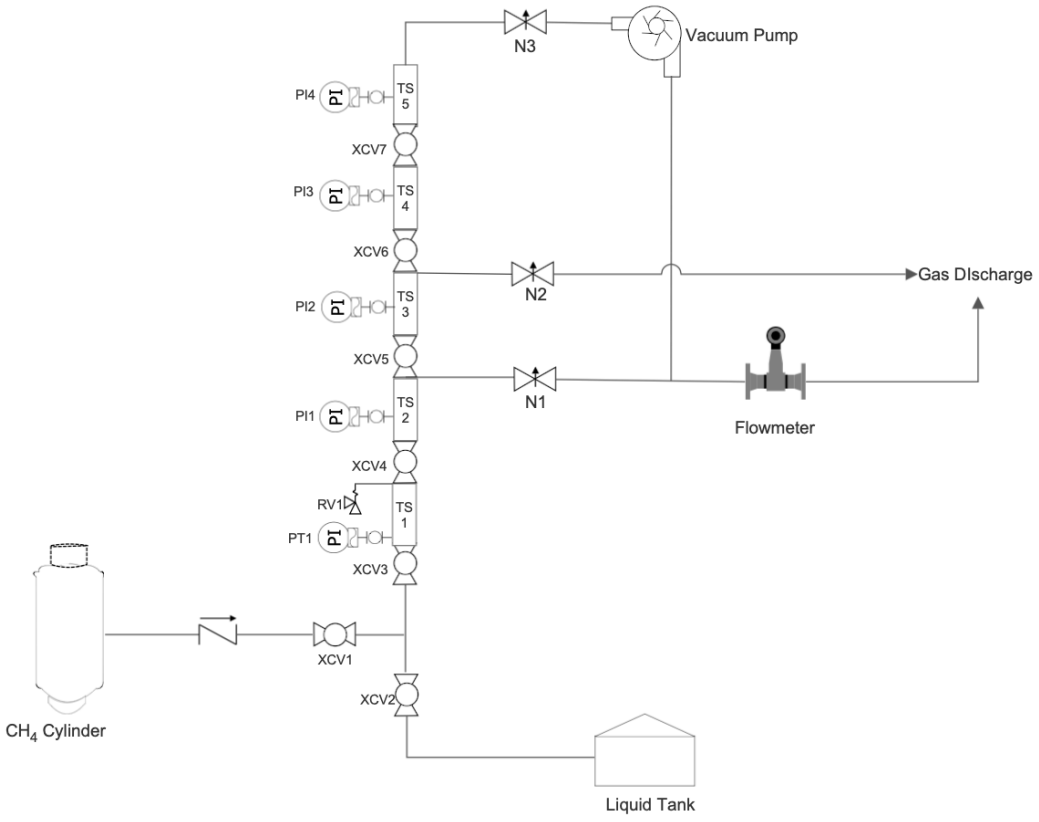

Figure 3.1. P&ID of the Low-Pressure Mass Transfer Apparatus

3.2. Experiments with peak outflow rate

The initial idea of the gas evolution experiments involved degassing the saturated liquid phase with the needle valve set at a desired peak flow rate of gas out of solution. A schematic of the peak flow rate experiments is shown in Figure 3.2. A ball valve is installed behind the needle valve for this methodology. In this experiment, the column was first filled with a known amount of the liquid phase. Methane was then flown through the liquid phase until complete saturation. Once saturation was confirmed using the pressure decay method, the needle valve, N1 at the end of TS2 was preset to the desired peak flowrate. XCV8 was then used to open/close flow of gas through the needle valve to the flow meter. To allow dissolved gas to evolve out of solution, XCV8 was completely

opened. Desorbed gas then flows through N1, and through XCV8 to the flowmeter due to differential pressure. To avoid an abrupt pressure drop in the TS1, the gas in TS2, with pressure up to that in TS1 was used as a blanket. This blanket gas ensured that the pressure drops gradually based on the degree of opening of N1. Equations A.4 and A.5 which account for the blanket gas were used to calculate the actual volume of gas that comes out of solution. (Details of the derivation are shown in Appendix A.1).

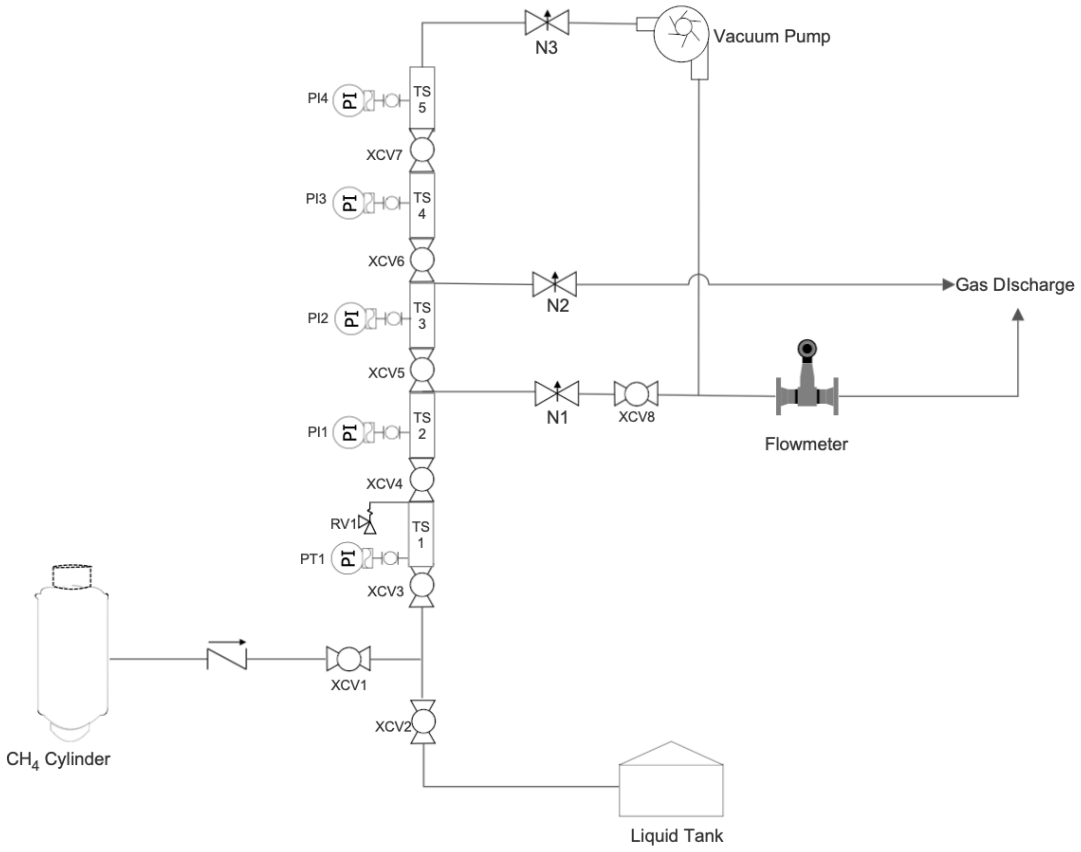

Figure 3.2. P&ID showing the configuration of the peak outflow rate experimental set up

Table B.1 presents the tests performed to investigate gas evolution using the peak flow rate methodology. Some of the results obtained using this method are shown in Figure 3.3. This figure describes the relationship between $K_L a$ and the peak flow rate at which the gas phase leaves the

apparatus at different initial saturation pressures. From the results, it is shown that the mass transfer coefficient increases with peak discharge flow rate. K_La increases with peak flow rate until it reaches an asymptotic value, where it becomes independent of the peak flowrates. As shown for each individual initial saturation pressures ranging from 0.69 MPa to 1.380 MPa (100-200 psi), K_La plateaus and becomes independent of the increasing peak flow rate. Figure 3.3 also illustrates that the asymptotic K_La value is reached at lower peak flow rates for tests with lower initial saturation pressures. This suggests that at higher initial saturation pressure, the flow rate where the K_La plateaus become higher.

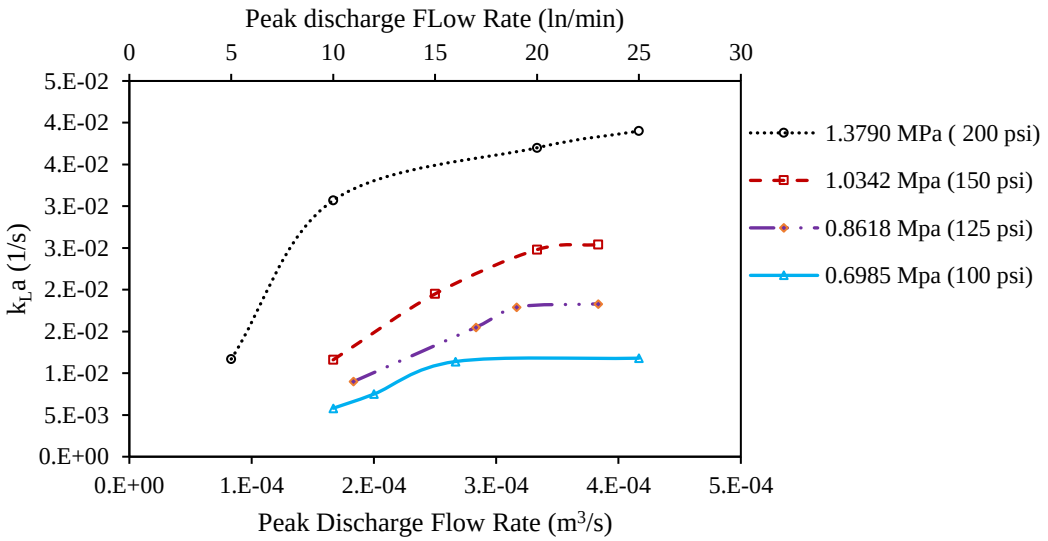

Figure 3.3. Desorption coefficient k_La as a function of peak discharge flow rates at pressures ranging from 0.69 to 1.380 MPa (100-200 psi) with diesel as the base oil

The capacity of the flow meter used for this experiment is 0.42×10^{-3} m^3/s (25 ln/min). Therefore, the desorption coefficient did not plateau for the 1.380 MPa (200psi) initial saturation pressure test before reaching the capacity of the flowmeter. The results for the lower pressure ranges suggested that if the apparatus had a flow meter with a higher capacity, the asymptotic mass transfer coefficient value would be reached for pressures at 1.380 MPa (200 psi) and above. We

did not however go further with this methodology because of the restriction due to the preset needle valve. As a result, a different methodology that had a lesser disruption to the degassing process was developed.

3.3. Experiments with Rapid Depressurization

Since the experiments with peak outflow rate restricted the flow of gas evolving from solution, the experiment had to be modified to the rapid depressurization methods to reduce the flow restriction caused by the preset needle valve. This methodology is similar to the one followed by Fortkamp(2014)(Fortkamp & Barbosa Jr, 2015), Blázquez (2016)(Blázquez et al., 2016), & Wang et al (2019)(Wang et al., 2019). A schematic of the rapid depressurization experiments is shown in Figure 3.4. Both the needle valve, N1 and Ball valve, XCV8 in Figure 3.3 are removed from the set up for this experiment. To perform the rapid depressurization experiment, a known volume of the liquid phase is fed into the column. Then gas was allowed to flow gradually through the first test section until complete saturation was attained in the test section. TS1, containing the saturated liquid was first isolated and methane was removed from the remaining test sections through N2 to the gas discharge. Then, XCV4 was rapidly opened to allow dissolved gas to evolve from solution due to depressurization. The pressure, totalized volume and evolved gas flow rate were recorded every 0.1 seconds by the Data acquisition system until flow had ceased. The acquired data was used to determine the dissolved gas concentration, C_L as a function of time. The dissolved gas concentration at the beginning of the experiment, C_o was determined by degassing the liquid in Test section 1 through vacuuming and adding the total degassed volume to the total volume that desorbed freely from solution.

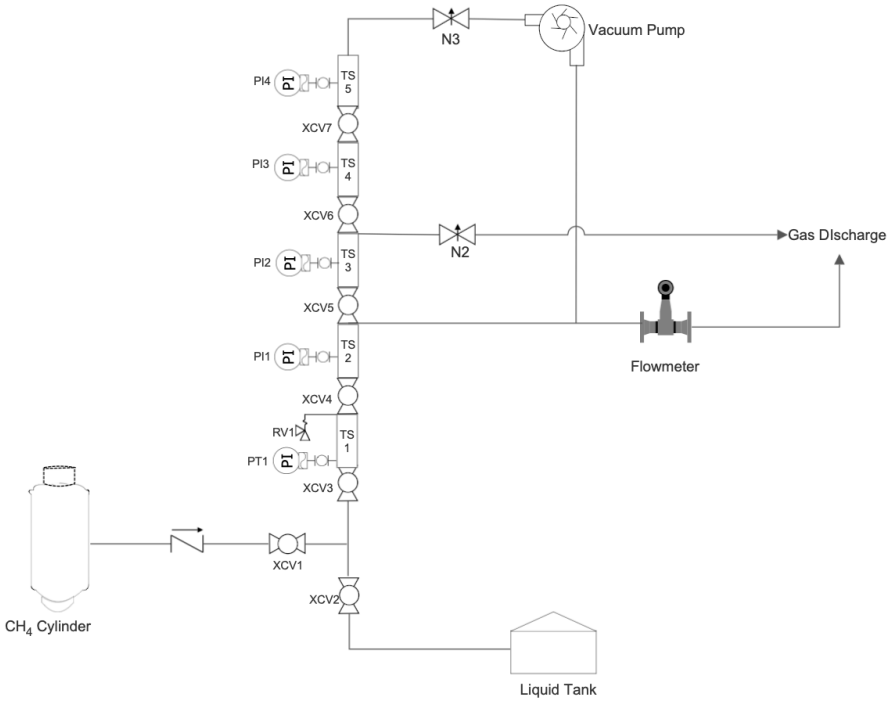

Figure 3.4. P&ID showing the configuration of the rapid depressurization experimental set up

The data obtained using this method were modeled using the instantaneous k_La which is further discussed in the modelling section in chapter 5. Some of the tests performed using this methodology are shown in Table B.2.These tests were used to confirm the time dependency of desorption that had previously been shown by other investigators (Hamborg et al., 2010; Huerta et al., 1996; Kierzkowska-Pawlak & Chacuk, 2010; Miranda et al., 2019; Sheng et al., 1999).

The time dependent desorption was illustrated by plotting the pressure drop from TS1 and the desorbed gas flow rate on the same plot. The latency in the measurement of desorbed gas by the flowmeter is accounted for using the mass balance equation shown in Eqn. 3.1 (Details of the derivation is shown in appendix C).

$$q_i = q_o + \frac{V_t}{P\Delta t}(P_t - P_{t=0}) \tag{3.1}$$

Where q_i is the actual flow rate of gas desorbing from liquid (ln/min), q_o is desorbed gas flow rate measured by the flow meter (ln/min), V_t is the volume of the first test section (liters), P_t is the Pressure of gas in the second test section at a specific time, (atm), $P_{t=0}$ Pressure in the second test at time t = 0, usually atmospheric pressure (atm) and Δt is the time step.

Figure 3.5 shows as desorption was initiated, the pressure of the solution dropped with time, whereas the desorbed gas flow rate attained a maximum and began to thin out over time. By comparing the two curves, it is observed that the pressure of the solution reaches 0 psig 13 seconds earlier than it takes the desorbed gas flow rate to reach 0 l/min.

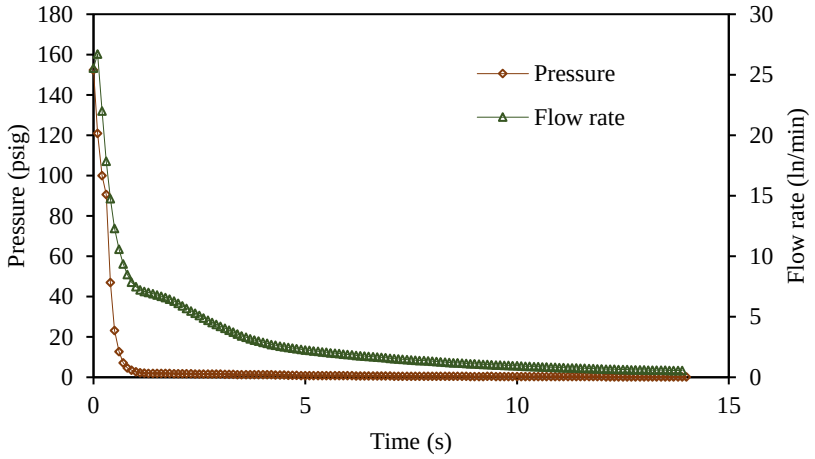

Figure 3.5. pressure and desorbed gas flow rate against time for internal olefin mixed with 2.5 wt.% suspentone to show the time dependency of desorption.

Pressure difference being the major driving force for the flow of desorbed gas, it would bne expected that the flow rate reaches zero almost immediately as the pressure of the system gets to zero psig. The reason for this considerable lag between the system's pressure and the desorbed gas

flow rate is due to desorption occurring even as the pressure of the system drops to zero. This illustrates that the desorption of gas is indeed not instantaneous, but time dependent.

However, the choked flow condition was encountered with the rapid depressurization experiment, where the gas velocity increases as it flows through smaller cross-sectional area of the constriction, which may result in overestimated gas outflow rate. It was also determined that the rapid depressurization methodology only simulates desorption that occurs at few instances during a well control event – such as when the kick exits the choke. But desorption could also occur during kick migration from the bottom of the well to the surface. Hence, an experimental method that reduces the possibility of choked flow and better simulates the desorption phenomenon that occurs during the majority of a well control scenario was established.

3.4. Experiments with Gradual Depressurization

Experiments with gradual depressurization was developed to remedy situations regarding choked flow and to better simulate the gas evolution phenomenon during drilling. The P&ID of the experimental apparatus during gradual depressurization experiments is shown in Figure 3.6. Only the needle valve, N1 is needed to control flow to the flow meter for this procedure. To perform this experiment, the apparatus was first vacuumed to ensure it was completely empty. Then 0.00053m^3 (530 ml) of Internal olefin was syphoned into the bottom of the vessel. Upon filling out part of the test section with liquid, the remaining section was further vacuumed to take out the remaining free gas. The initial pressurization stage starts by pressurizing the system to the desired initial saturation pressure using the methane cylinder. The absorption stage was initiated by flowing methane through the liquid in the first test section for each experiment until complete saturation is attained in the test section. After complete saturation was confirmed using the

pressure decay method, the system was depressurized gradually by controlling the needle valve, N1 from the initial saturation pressure to atmospheric pressure. The void space between the gas liquid interface and the flowmeter via the needle valve holds some gas during the entire depressurization stage. This volume has been accounted for in the gas evolution calculation with the help of the formula derived shown in appendix A. Due to depressurization, gas evolves from the liquid until a new equilibrium is reached. The flow rate and total volume of evolved gas were recorded every 0.2 seconds by the Data acquisition system.

The acquired data was then used to determine the dissolved gas concentration, C_L as a function of time. The initial dissolved gas concentration, C_o was obtained by degassing the liquid phase through vacuuming and adding the total degassed volume to the total volume that evolved from solution during desorption. The gradual depressurization method was used in the remainder of the study to investigate gas evolution of methane from saturated base fluids.

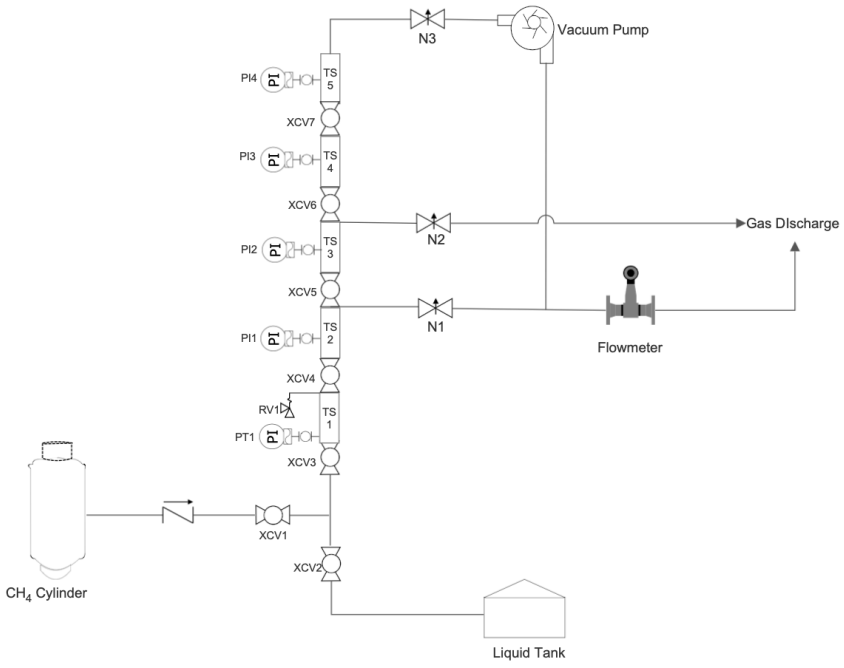

Figure 3.6. P&ID showing the configuration of the gradual depressurization experimental set up

3.5. Summary

The experimental methodology was continually modified from peak flow rate experiments to rapid depressurization experiments, then gradual depressurization experiments. By modifying from peak flow rate experiments to rapid depressurization experiments, the restriction to the flow of gas was avoided. Then changing to the gradual depressurization prevented choked flow and helped to better simulate the desorption that is expected throughout the length of the drilling/riser column. The gradual depressurization methodology was utilized in the remainder of the experiment to investigate gas evolution.

CHAPTER 4. DESORPTION EXPERIMENTS

4.1. Materials

Two different types of non-aqueous based fluids were used in this study: Diesel and Olefins. The physical properties of each fluid are provided in Table 4.1. The diesel used in this study is a standard blended diesel used for both oil-based drilling fluids and for automotive use, known as No. 2 Diesel Fuel. This fluid is subject to EPA regulations on the sulfur content of <15 ppm and consists of carbon numbers generally between C9-C23 in weight. The olefins have molecular chain lengths between C10-C24 used in the field for drilling fluid development. GC-MS analysis results of the internal olefin used in this investigation is provided in Table 4.2. Lastly, Methane with 99% purity was used as the gas phase in this study.

Table 4.1. Physical properties of Diesel and Olefins.

Fluid	Density (kg/m^3)	Viscosity (40 °mm^2/s)	Aniline Point (°C)	Sulfur Content (mol/m^3)	Color
Diesel	831.95	2.1	49	<14.08	Yellow
EDC 99-DW US Olefins	815.90	2.4	79	<0.028	Clear

The olefins were characterized using Gas Chromatography-Mass Spectrometry (GC-MS) analysis by following the procedure discussed here. The analysis was carried out with gas chromatography, model GC-6890N coupled with mass spectrometer, model MS-5973 MSD (mass selective detector). A capillary column DB-5MS (30 m× 0.32 mm, 0.25 μm of film thickness) was used for the separation and helium was used as the carrier gas with a flow rate of 1.5 mL/min. The temperature of the column was programmed from 80 to 300 °C at a rate of 5 °C/min. Both the injector and detector were set at a temperature of 250 °C. Using a split ratio of 1:10, a 20 μLvolume

of olefins diluted with heptane was injected using a split mode. The mass spectrometer was set to scan in the range of m/z 50–550 with an electron impact (EI) mode of ionization.

Table 4.2. GC-MS Analysis results of identifiable compounds within the internal olefin sample.

Compound	Location of C=C bonds	Carbon Chain Length
Decane		10
Tridecane		13
Tridecene	1,	13
Tetradecane		14
Tetradecene	2, 3, 5, 6	14
Hexadecane		16
Hexadecene	7	16
Heptadecene	3, 8	17
Octadecene	3, 5	18
Nonadecene	1, 5	19

As shown in Table 2, the Gas Chromatography-Mass Spectrometry analysis carried out indicates that the olefins tested in this study ranged from C10-C19. The analysis also showed that there were measurable levels of linear alpha olefins 1-Tridecene and 1-Nonadecene and saturated hydrocarbon chains, decane, tridecane, tetradecane, and hexadecane.

4.2. Development and Surface Tension Measurement of Fluids

A known volume of olefins was first transferred into the blender. The blender was turned on and 2.5 % volume of span 80 by volume of the liquid phase was added to the liquid. The system was vigorously shaken for about 5 mins to ensure complete mixing of the surfactant with the oil

phase. Water was then slowly added to the oil phase to ensure homogenous distributions of the water droplets. The emulsions were then further homogenized using an ultrasonicator shown in Figure 4.1 for 5 mins with a 40% amplitude, 25s on, 15s off pulse

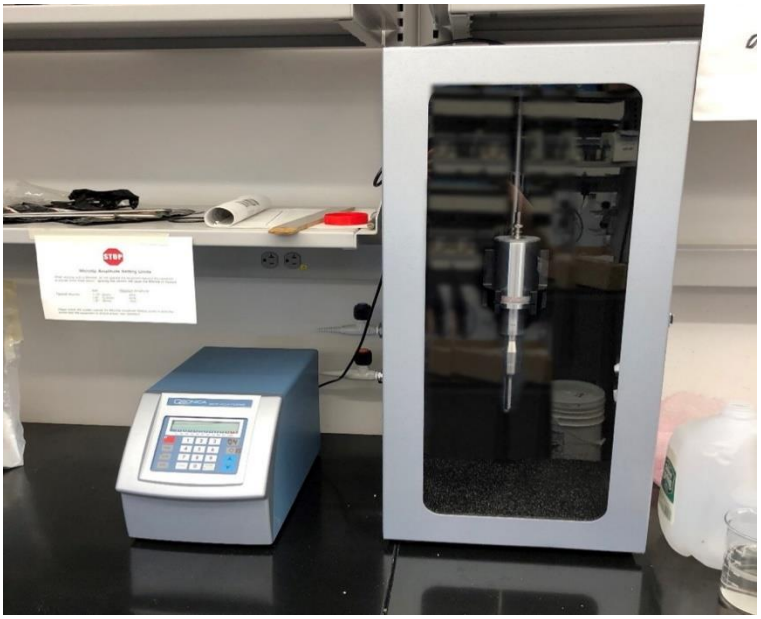

Figure 4.1. Q-Sonica Q500 Ultrasonicator

The surface tension measurements were taken at atmospheric pressure (0.101325 MPa) and ambient temperature (25°C).

Table 4.3. Interfacial tension measurements

Fluids	Density (g/cm^3)	Mean IFT value (mN/m)	Standard Deviation
Pure Internal Olefin-air	0.816	38.13	0.020
Internal olefin with span 80-air	0.824	38.19	0.064

The density of Olefins at those pressure and temperature conditions were 0.816 g/cm^3 and these values were utilized for the measurements. The measurements were carried out using an interfacial

tensiometer. Repeated measurements were taken, and the reported values given in Table 4.3 are average values of more than 50 reading

4.3. Development and Viscosity measurements of Viscous Fluids

The viscous fluids were prepared using a mechanical blender operating for 5 min at a high speed. The viscous fluids were made by mixing a wt.% of suspentone by volume of liquid with a specific volume of internal olefin.

The viscosity of the fluids investigated were obtained using a Rheometer, and the resulting viscosity and yield points are presented in Table 4.4. The yield point increases with the concentration of suspentone.

Table 4.4. Flow properties of the fluids investigated

Fluid	Yield point (pa)
Pure Internal Olefin	0
IO with 5% suspentone	43.9

4.4. Design of Experiments

In this study, experiments were conducted to understand the effect of initial saturation pressure, depressurization rate, oil-water ratio of emulsion, different liquid phases, addition of viscosifier and presence of surfactant on gas evolution. Tables 4.5 and 4.6 show the experimental designs for the parameters investigated. All tests were conducted twice to check the repeatability of the experiments. The tests shown in Table 3 were conducted to investigate the effect of initial

saturation pressure and depressurization rate on gas evolution. To investigate the effect of Initial saturation pressures on desorption, experiments were conducted with initial saturation pressures ranging from 0.69(100) to 2.07 MPa (300psi) at constant depressurization rates of 0.0034 and 0.0103 MPa/s (0.25 and 1.5 psi/s).

Table 4.5. Test matrix to investigate the effect of initial saturation pressure and depressurization rate on gas evolution

S/n	Fluid System	Initial Saturation Pressure (MPa)	Initial Saturation Pressure (psi)	Depressurization rate (MPa/s)	Depressurization rate (psi/s)
1	Methane/IO	0.69	100	0.0034	0.5
2				0.0103	1.5
3		1.38	200	0.0017	0.25
4				0.0034	0.5
5				0.0103	1.5
6				0.0276	4
7				0.0551	8
8				0.1724	25
9				0.6895	100
10		2.07	300	0.0034	0.5
11				0.0103	1.5

Whereas 7 different depressurization rates, ranging from 0.0017 to 0.6895 MPa/s (0.25 to 100 psi/s) were varied at a constant initial saturation pressure of 1.38 MPa to study the effect of depressurization rate on gas evolution.

Table 4.6 shows the tests that were conducted to investigate the effect of different liquid phases and oil water ratio of emulsion on gas evolution. The tests were all conducted with an initial

saturation pressure of 1.38 MPa (200 psi) and a depressurization rate of 0.00689 MPa/s (1psi/s). Internal olefin and diesel are the most used non-aqueous based fluid in the drilling industry. As a result, the behavior of gas evolution from these two fluids were compared. 50-50 Internal olefin – water emulsion was used to evaluate the effect of having emulsion as the liquid phase. A surfactant concentration of 2 vol. % by volume of liquid was used to study the effect of surfactant on mass transfer, while a suspentone concentration of 5wt% by volume of liquid was used to elucidate the effect of viscosifying agents on gas evolution. Tests 1, 3 and 4 of Table 4.6 were used to elucidate the effect of oil water ratio of emulsion of gas evolution.

Table 4.6: Tests to study gas evolution for different fluids.

s/n	Pressure, MPa (psi)	Trials	Depressurization rate, MPa/s (psi/s)	Tests
1	1.38 (200)	2	0.00689 (1)	Pure Internal Olefin
2				Pure IO mixed with 2% span 80
3				70:30 IO/W emulsion
4				50:50 IO/W emulsion
5				Diesel
6				IO mixed with 5% suspentone

4.6. Summary

The materials and the formulation of the liquid phases that were used in conducting the gas evolution experiments were presented here. The surface tension and viscosity measurements shown in this chapter is crucial in explaining some observations made in the results section. Finally, the test matrix followed to investigate the effect of initial saturation pressure,

depressurization rate, presence of surfactant, different liquid phases, and oil water ratio on gas evolution were shown.

CHAPTER 5. MODELLING AND RESULTS OF DESORPTION EXPERIMENTS

Desorption data were obtained using the gradual depressurization methodology explained in Chapter 3. The task now is to analyze this data to obtain useful results. This chapter provides the models that were tested to characterize the desorption experiments, the model that was eventually employed and the results obtained using this model.

5.1. Modelling of Desorption Experiments

Two methods of analyzing the gas evolution data were attempted in this study.

1. Overall Volumetric Mass Transfer Coefficient
2. Instantaneous Volumetric Mass Transfer Coefficient

5.1.1 Overall Volumetric Mass Transfer Coefficient

As discussed in section 2.4, few models have been proposed to study the desorption kinetics of gas from a solution. Tunnat et al, (2014)(Tunnat et al., 2014) examined the desorption of CO_2 from water and aqueous amine solutions using a two-film theory as given in Eqn. 2.9.

From their findings, the simple two-film model represents accurately the desorption process of carbon dioxide from a simple physical solvent such as water. The applicability of this model to our experiment was evaluated, and it was seen that the presence of two unknowns, gas, and liquid mass transfer coefficient (k_g and k_L) complicates the use of the model with our experimental data.

A model which relates the rate of gas transfer from a liquid phase to the difference between saturation concentration (C_s) and the existing concentration of gas (C_L), $C_L - C_S$ (Lewis & Whitman, 1924) as given in Eqn. 2.3 was tested with our experimental data. This equation has been used by several studies to describe the mass transfer process of gas desorbing from liquids.

(Barrut et al., 2012; Alden B Daniel et al., 2019; Eshchar et al., 2003; Lisitsin et al., 2008; Miranda et al., 2019)

The volumetric mass transfer coefficient is then given as the slope of the linear fit of $\ln\left(\frac{C_s - C_o}{C_s - C_L}\right)$ vs time. Applying this model to the data obtained from the gradual depressurization tests yielded a straight line, whose slope was taken as the overall volumetric mass transfer coefficient. However, applying this model to the rapid depressurization experimental data yielded a curve, which led to analyzing the data from the rapid depressurization experiments with instantaneous mass transfer coefficient as described below.

5.1.2. Instantaneous k_La

Applying Eqn. 2.4 to data obtained from the rapid depressurization experiments, the existence of two regions was observed as shown in Figure 5.1. From the figure, the initial stage of desorption named bubble desorption corresponds to high values of supersaturation. As desorption occurs, the supersaturation decreases. In this region of reduced supersaturation, the mass transfer takes place by a diffusive mechanism. The observations made here were in agreement with those made by Weiland et al (1977) (Thuy & Weiland, 1976)(Figure 5.2) and, Hikita and Konishi (1984)(Hikita & Konishi, 1984). Weiland et al (1977) suggested that this change in the mass transfer coefficient is due to a mechanism change from bubble desorption to quiescent desorption.

This section was previously published as Ojedeji D, Perry S, Nielsen J, Chen Y. "Experimental investigation of desorption kinetics of methane in diesel and internal olefin for enhanced well control", Greenhouse Gases: Science and Technology. 2020;10(2):364-79. Reprinted by permission of Wiley Press.

As presented in Figure 5.1, the slope of the graph, which represents the mass transfer coefficient starts to change at about three seconds. This point is regarded as the transition point from bubble to quiescent desorption. Investigators could take the slope of bubble desorption period as the desorption coefficient (see Figure 5.1).However, the transition curve between bubble and quiescent desorption makes selecting the endpoint of bubble desorption highly subjective and this may lead to erroneous estimation of the mass transfer coefficient. To address this problem, an instantaneous mass transfer coefficient, [$K_L a$] was obtained using a time marching analysis, [$K_L a$]. Eqn. 2.4 was assumed to be valid for this short instance of time, therefore, the mass transfer coefficient was assumed to be constant. Also, the time marching analysis utilizes the instantaneous gas bulk and interfacial concentrations, C_L and C_s in calculating the [$K_L a$] value for each time step, t. Different $K_L a$ values were obtained every 0.1s for a period of 5 seconds, and it was observed that the instantaneous mass tranafer coefficient decreased with time as shown in Figure 5.3.

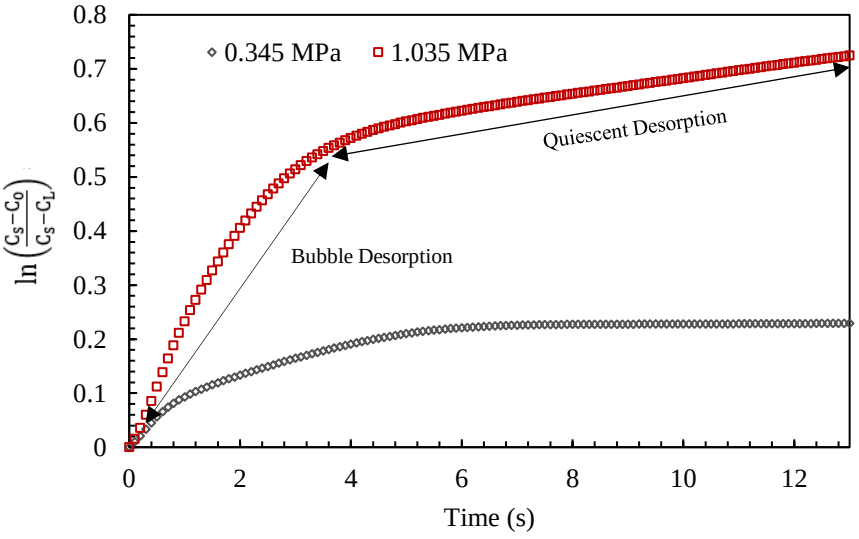

Figure 5.1. $\ln\left(\frac{c_s-c_o}{c_s-c_l}\right)$ vs time for internal olefin with an initial saturation pressures of 0.345 MPa and 1.035 MPa showing changes in the overall mass transfer coefficient overtime

This decrease in the instantaneous mass transfer coefficient could be attributed to a decrease in the level of oversaturation as desorption occurs. The $[K_La]$ approaches zero where there is no considerable desorption of methane from the liquid phase. As $[K_La]$ changes over time for the rapid depressurization experiments, it was necessary to find a value that most characterizes the gas evolution behavior of the system.

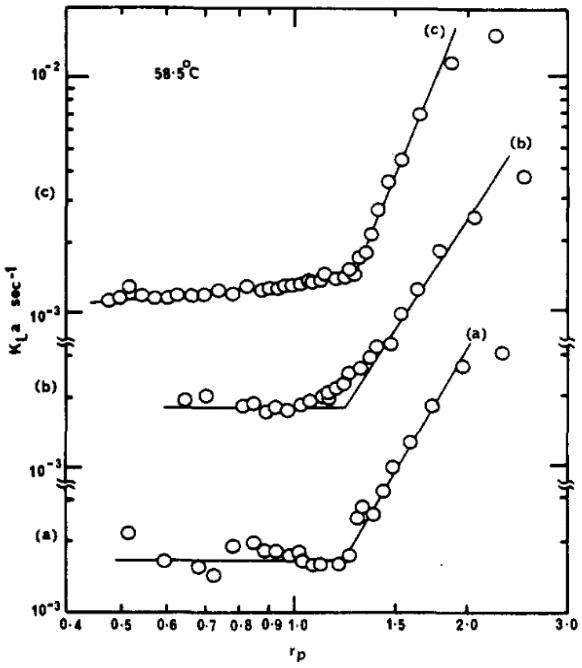

Figure 5.2. Variation of mass transfer coefficient with the pressure-reduction ratio for three experiments conducted by Welland et. al, 1977

Consequently, the maximum instantaneous mass transfer coefficient, $[K_La]_{max}$ which corresponds with the period where the most drastic desorption occurs was used to describe the desorption process for a system of fluids for the rapid depressurization experiments. However, estimating instantaneous desorption coefficient requires highly accurate measurements. Minor

inaccuracies in the measurement or during the procedure marred the mass transfer coefficient values obtained from the time marching analysis.

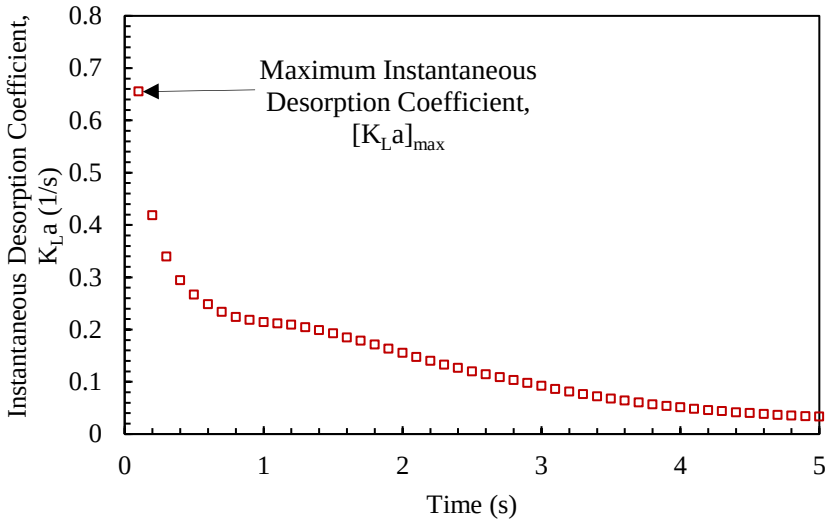

Figure 5.3. Instantaneous Desorption Coefficient for internal olefin with an initial saturation pressure of 1.035 MPa (150 psi)

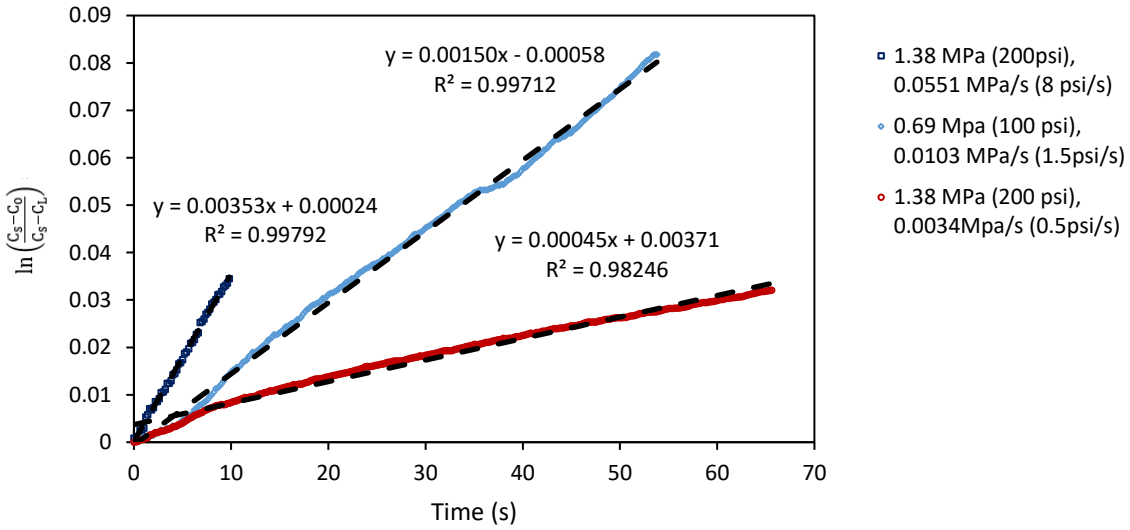

Figure 5.4. $\ln\left(\frac{C_s-C_o}{C_s-C_L}\right)$ vs time for desorption at 1.38 MPa (200 psi) and 0.0551 MPa/s (8 psi/s), 0.69MPa (100 psi) and 0.0103MPa/s (1.5psi/s), 1.38 MPa (200 psi), 0.0034 MPa/s (0.5 psi/s)

Hence, to circumvent this problem, the overall volumetric mass transfer coefficient, which uses Eqn. 2.4 was utilized for the remainder of this study to describe the experimental data. Figure 5.4 is an example of the plots when Eqn. 2.4 was applied to the gradual depressurization experimental data. The resulting linear fit yielded a slope of 0.0015 1/s and an R^2 value of 0.9971 for desorption experiment carried out at an initial saturation pressure of 0.69 MPa (100 psi) and depressurization rate of 0.0103 MPa/s (1.5 psi/s).

5.2. Error Propagation

Monte Carlo error propagation technique was used to estimate the experimental error in the gas evolution experiments in this study. The sources error used in this evaluation were from the pressure transducer, flow meter and measuring cylinder. The measurements from the pressure transducer, flow meter and measuring cylinder had an uncertainty of σ_p $\pm$1% of RD, σ_q $\pm$1% of RD, and σ_{V_L} $\pm$1ml respectively. It was assumed that the uncertainty between the pressure, flow meter and measuring cylinder were uncorrelated.

First a gaussian distribution was generated using Box-Muller transform given in equation 5.1

$$f_{gauss}(X_1, X_2) = \sqrt{-2 \ln X_1} \cos 2\pi X_2 \tag{5.1}$$

Where, X_1 and X_2 were independently generated random numbers ranging from 0 to 1. The gaussian distribution was then used to add a normally distributed noise to the measured variables as shown in Eqns. 5.12, 5.3 and 5.4.

$$P_\sigma = f_{gauss}(X_1, X_2)\sigma_p + P \tag{5.2}$$

$$q_\sigma = f_{gauss}(X_1, X_2)\sigma_q + q \tag{5.3}$$

$$V_{L_\sigma} = f_{gauss}(X_1, X_2)\sigma_{V_L} + V_L \tag{5.4}$$

Once the measured values with their associated distribution are generated, they can then be used to propagate the error through other calculations.

The distribution in the calculated total evolved gas volume was evaluated using Eqn. 5.5

$$V_{T_\sigma} = f(q_\sigma) \tag{5.5}$$

The distribution in the corrected total evolved gas volume was then obtained using equation A.4 and A.5, which accounts for the blanket gas volume as shown in Eqn. 5.6.

$$V_\sigma = f(V_{T_\sigma}, q_\sigma, P_\sigma) \tag{5.6}$$

Once the corrected volume is evaluated, the distribution of the concentration of methane in the liquid phase is then evaluated using Eqn. 5.7

$$C_{L_\sigma} = \frac{EOS(P_\sigma, T, V_\sigma)}{V_{L_\sigma}} \tag{5.7}$$

Figures 5.5, 5.6 and 5.7 shows the gas evolution profile for different conditions along with the experimental uncertainty associated with them.

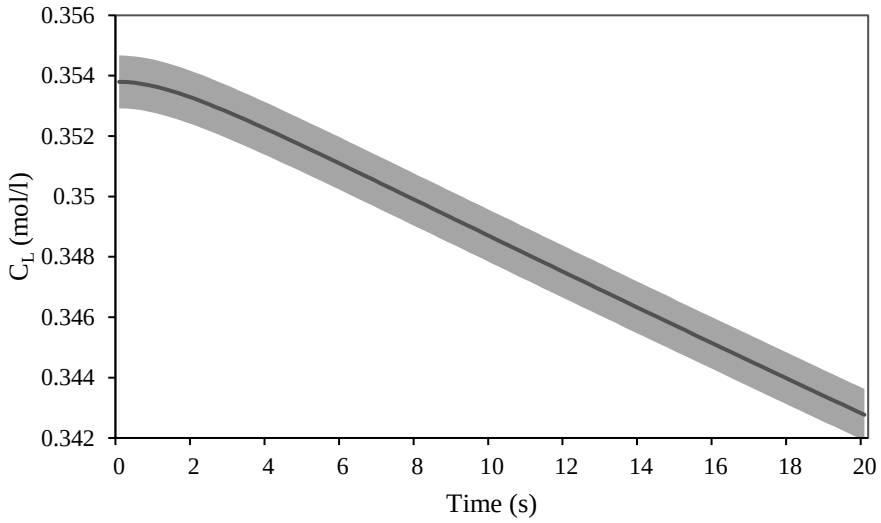

Figure 5.5. Concentration of methane in internal olefin during desorption for initial saturation pressures of 1.38 MPa (200 psi) constant depressurization rate of 0.0034 MPa/s (0.5 psi/s). The solid line is the measured concentration, whereas the shaded region shows the uncertainty in the measurement.

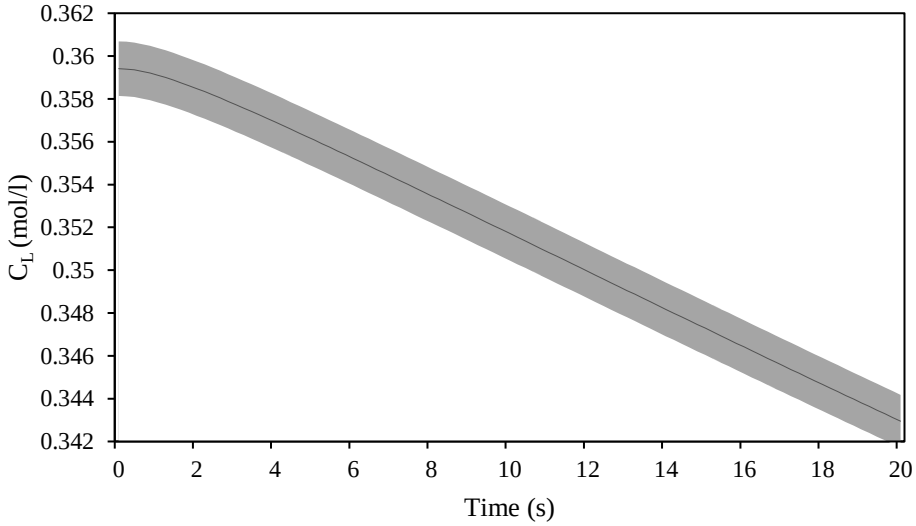

Figure 5.6. Concentration of methane in internal olefin during desorption for initial saturation pressures of 1.38 MPa (200 psi) constant depressurization rate of 0.0103 MPa/s (1.5 psi/s). The solid line is the measured concentration, whereas the shaded region shows the uncertainty in the measurement.

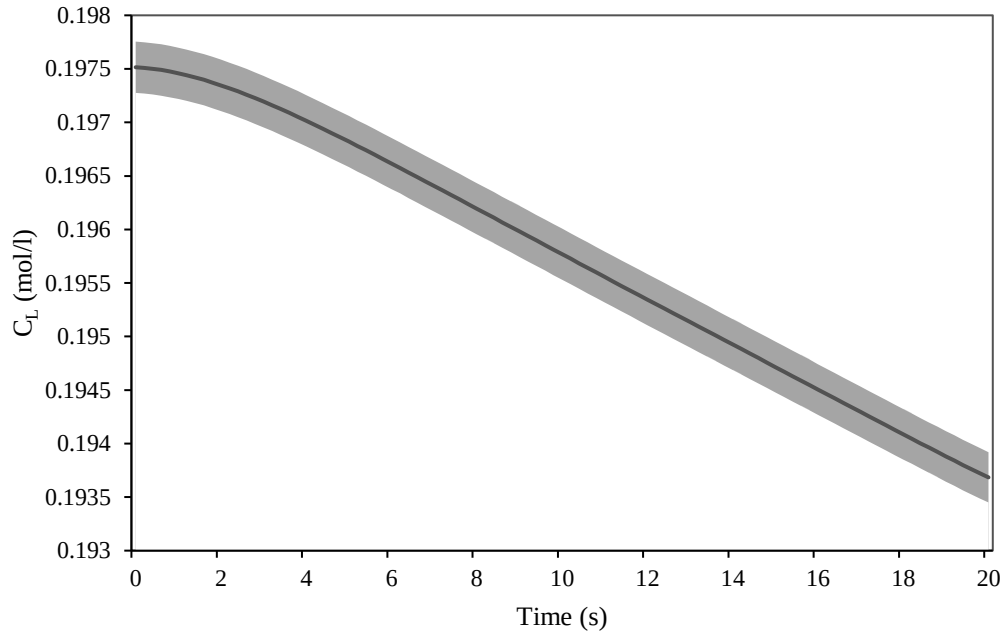

Figure 5.7. Concentration of methane in internal olefin during desorption for initial saturation pressures of 0.69 MPa (100 psi) constant depressurization rate of 0.0034 MPa/s (0.5 psi/s). The solid line is the measured concentration, whereas the shaded region shows the uncertainty in the measurement.

5.3. Results

The effects of initial saturation pressure, depressurization rate, different liquid phases, and oil-water ratio of emulsion on gas evolution are discussed in this section

5.3.1. Effect of Initial Saturation Pressure on Gas Evolution

Gas evolution experiments were conducted at three different initial saturation pressures – 0.69, 1.38 and 2.07 MPa (100, 200, and 300 psi) to investigate the effect of the initial saturation pressure. These experiments were repeated for two different depressurization rates, while keeping other parameters such as temperature, fluid type, and liquid height constant. According to Henry's law, an increase in pressure increases the amount of gas dissolved in a liquid phase which is confirmed

by Figure 5.8, where the amount of methane that dissolves in internal olefin increases linearly with initial saturation pressure.

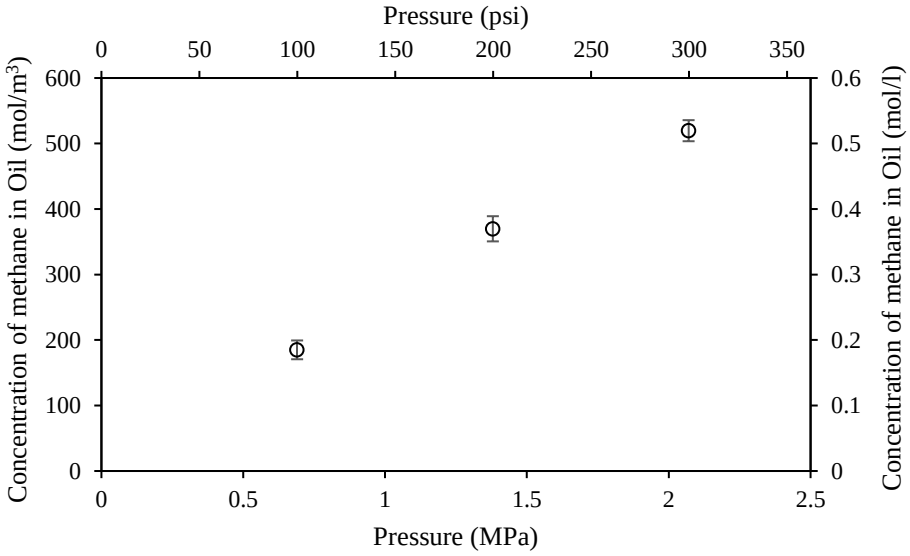

Figure 5.8. Dissolved methane concentration in internal olefin at varying initial saturation pressures

Figure 5.9 shows the variation of the concentration of methane in Olefin with time for different initial saturation pressures. Methane concentration decreases with time for all initial saturation pressure which indicates the desorption of gas out of solution. The concentration decreases for all initial saturation pressures at approximately the same rate, 0.45 ($\pm$0.05 mol/m^3/s), which was due to the same depressurization rate used for each experiment.

The effect of initial saturation pressures on the volumetric mass transfer coefficient (k_La) at two different depressurization rates, 0.0034 and 0.0103 MPa/s (0.5 and 1.5 psi/s) are shown in Figure 5.10.

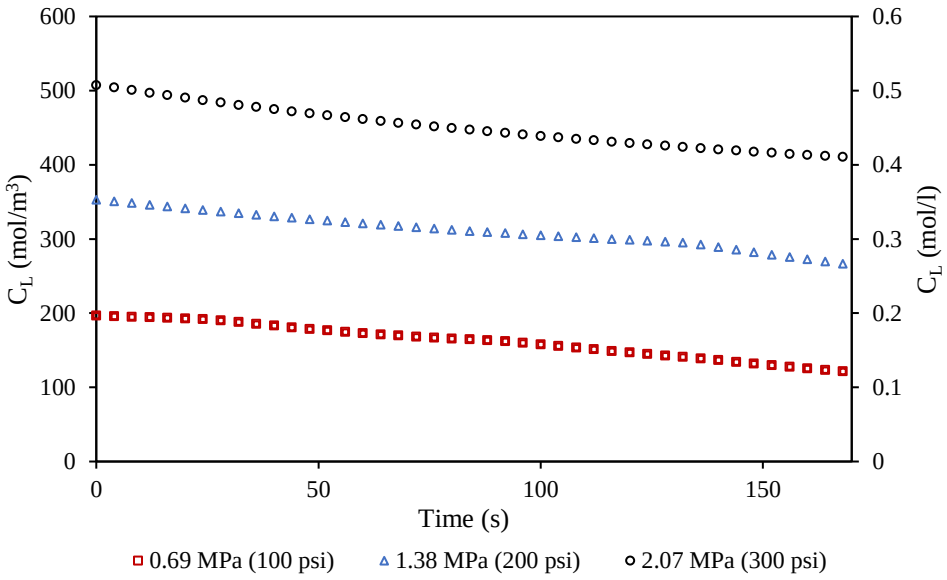

Figure 5.9. Concentration of methane in internal olefin during desorption for initial saturation pressures of 0.69 (100), 1.38 (200) and 2.07 MPa (300 psi) and constant depressurization rate of 0.0034 MPa/s (0.5 psi/s).

At a constant depressurization rate, the mass transfer coefficient decreases with initial saturation pressure within the range of initial saturation pressures investigated in this study. Daniel et al concluded that the mass transfer coefficient does not have a definite relationship with initial saturation pressure, which is different from the results presented here. The difference in the conclusion could be due to varying methodologies. In their case, mass transfer occurred predominantly through the interface, as opposed to mass transfer occurring through both the interface and the bubbles formed in this study. Therefore, decrease in the bubble size due to increased initial saturation pressure could be the reason for a lower mass transfer coefficient for higher initial saturation pressures

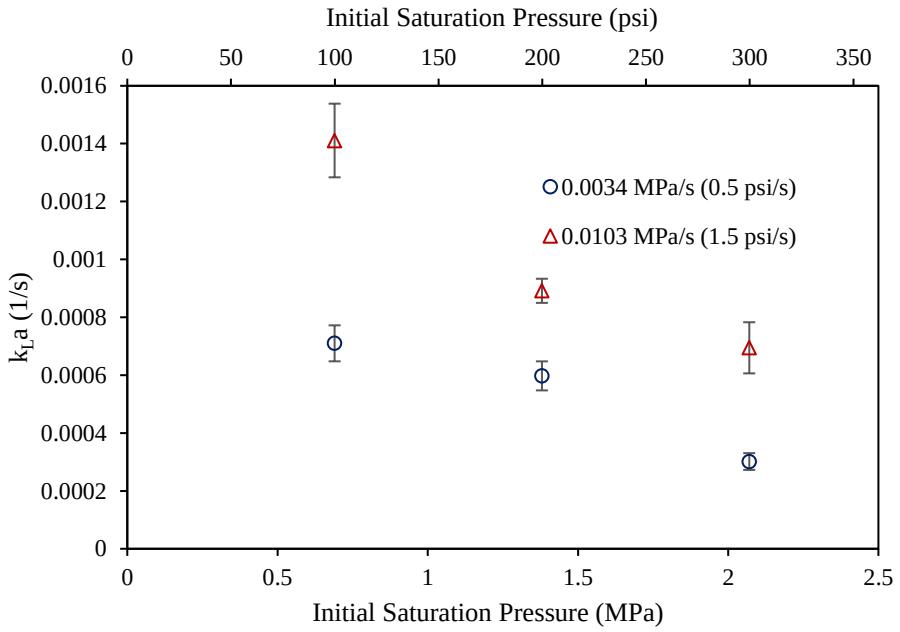

Figure 5.10. Effect of initial saturation pressure on the volumetric mass transfer coefficient at depressurization rates of 0.0034 MPa/s (0.5 psi/s) and 0.0103 MPa/s (1.5 psi/s)

5.3.2. Effect of Depressurization rate on Gas Evolution

To examine the effect of depressurization rate on the overall volumetric mass transfer coefficient, gas evolution experiments were conducted at three different initial saturation pressures, 0.69, 1.38, and 2.07 MPa (100, 200, and 300 psi) for depressurization rates of 0.0034 and 0.0103 MPa/s (0.5 and 1.5 psi/s). For all initial saturation pressures, increasing the depressurization rate led to an increase in the volumetric mass transfer coefficient as shown in Figure 5.11. The test matrix was extended to a wider range of depressurization rates to further investigate the effect of depressurization rates on the overall mass transfer coefficient. Experiments were performed ranging from a low depressurization rate of 0.0017 MPa/s (0.25 psi/s), which is typical of a well control scenario to rapid depressurization rates of 0.6896 MPa/s (100 psi/s), with the same initial saturation pressure of 1.38 MPa (200psi). Figure 5.10 shows the cumulative volume of evolved gas from Olefins for depressurization rates of 0.0034, 0.0103, and 0.0276

MPa/s (0.5, 1.5, and 4 psi/s) respectively. The cumulative volume of desorbed gas increases with time as gas evolution occurs. As expected, the rate of gas evolution increases as the depressurization rate increases. This is owing to a higher driving force, $C_L - C_s$ created by a faster depressurization as desorption takes place.

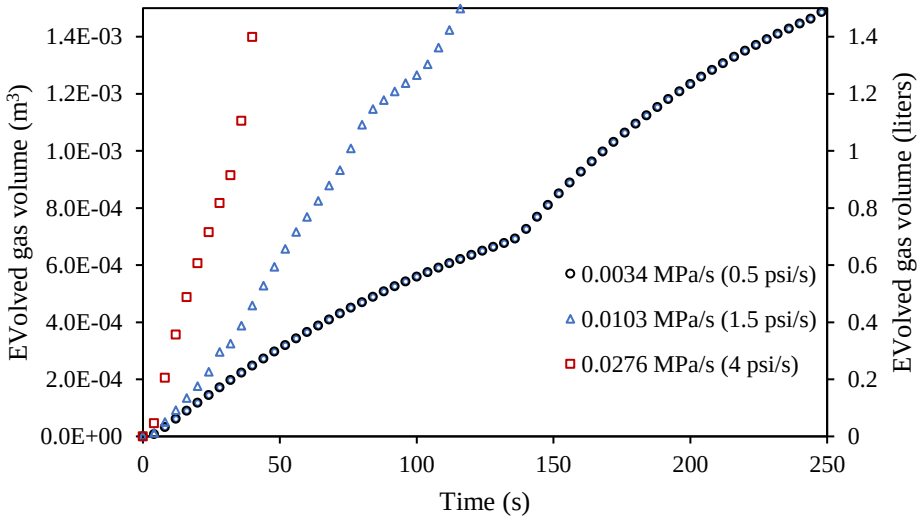

Figure 5.11. Volume of methane evolved at different depressurization rates (initial saturation pressure, 1.38 MPa (200 psi))

Figure 5.12 demonstrates the methane concentration variation in the liquid with time at various depressurization rates. While the initial concentrations for all three depressurization rates are the same owing to the same initial saturation pressure and hence the same amount of dissolved gas, the higher the depressurization rate, the faster the concentrations dropped. Figure 5.13 shows the volumetric mass transfer coefficient obtained for different depressurization rates. The mass transfer coefficients shown in cross markers are coefficients for higher depressurization rates, 0.1724 and 0.6895 MPa/s (25 and 100 psi/s) obtained from rapid depressurization experiments.

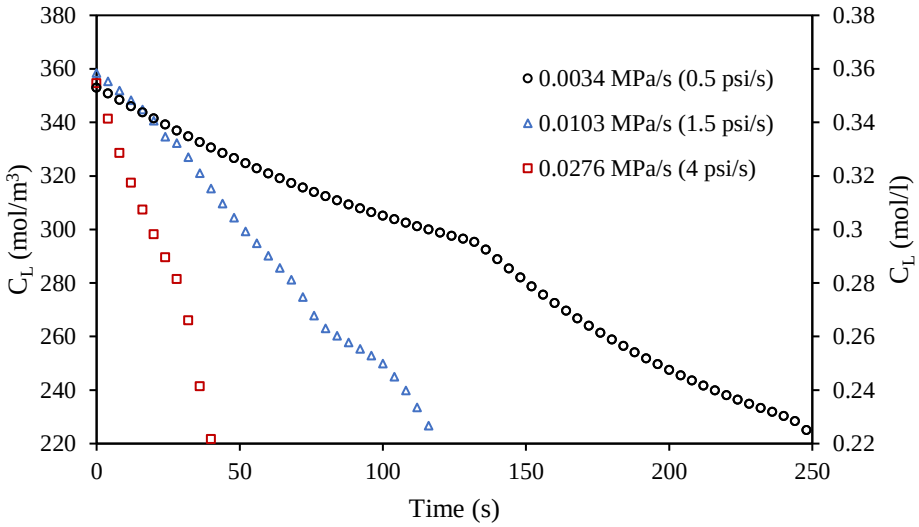

Figure 5.12. Concentration of methane in internal olefin during desorption for depressurization rates of 0.0034, (0.5), 0.00103 (1.5) and 0.0276 MPa/s (4 psi/s) and initial saturation of 1.38 MPa (200 psi)

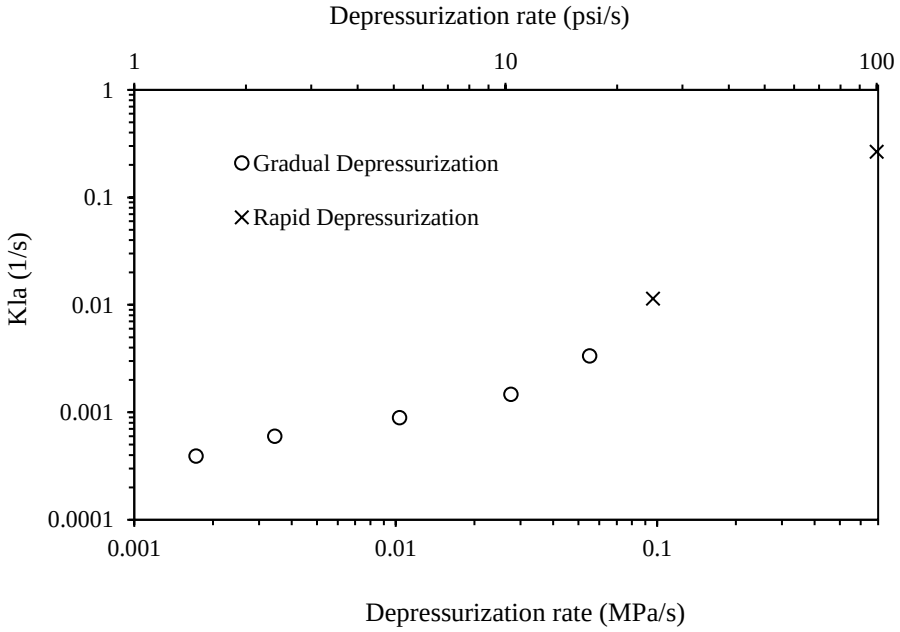

Figure 5.13. Effect of depressurization rate on volumetric mass transfer coefficient (initial saturation pressure, 1.38 MPa (200 psi))

Figure 5.13 confirms that the mass transfer coefficient increases with the depressurization rate. The increase may be attributed to higher bubble frequency resulting from a faster depressurization rate.

5.3.3. Effect of different liquid phases on gas evolution

Figure 5.14 shows the initial amount of methane dissolved in the liquid phase for different fluids considered in this study. From Figure 5.14, it is observed that the presence of surfactant does not significantly affect the solubility of methane in Olefin within the surfactant concentration investigated in this study. The solubility of methane in emulsion reduces compared to pure Olefin due to the lower capacity of methane to dissolve in the water phase, which is in agreement with the literature(Gevantman, 2000). The viscous fluid, which comprised of 5wt.% by volume of Olefin, dissolved just a little less than pure Olefin due to the presence of the viscosifying agent, suspentone. Of all 5 fluids investigated in this study, diesel had the highest capacity to dissolve methane.

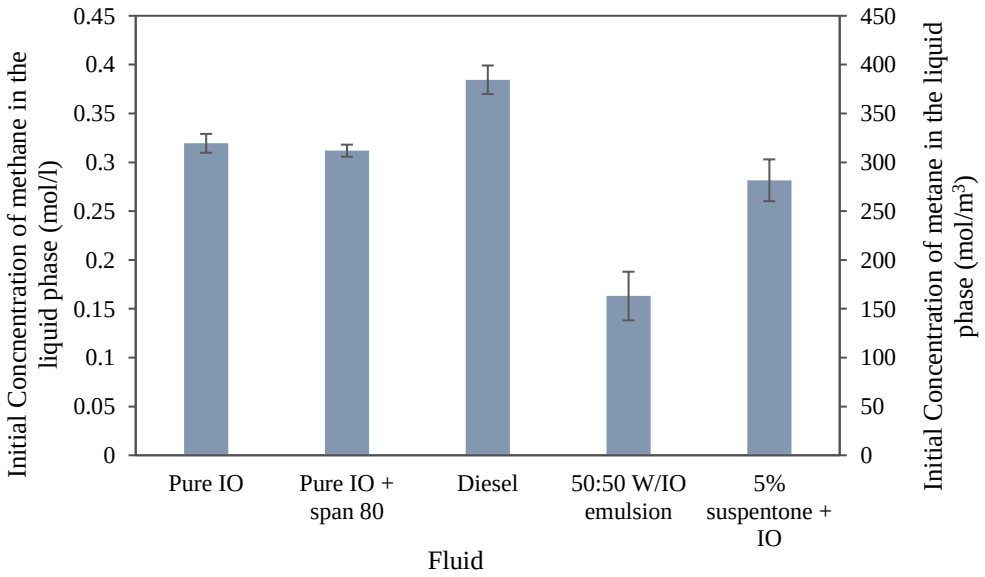

Figure 5.14. Dissolved methane concentration for different liquid phases.

Figure 5.15 presents the cumulative volume of methane evolved from different fluids compared to pure Olefins when the system is depressurized at a constant rate of 0.00689 MPa/s (1psi/s). From Figure 5.15a, the rate of methane evolution from both Olefins and Olefins mixed with span 80 were fairly the same, suggesting that the presence of surfactant does not significantly affect gas evolution rates of methane from olefins.

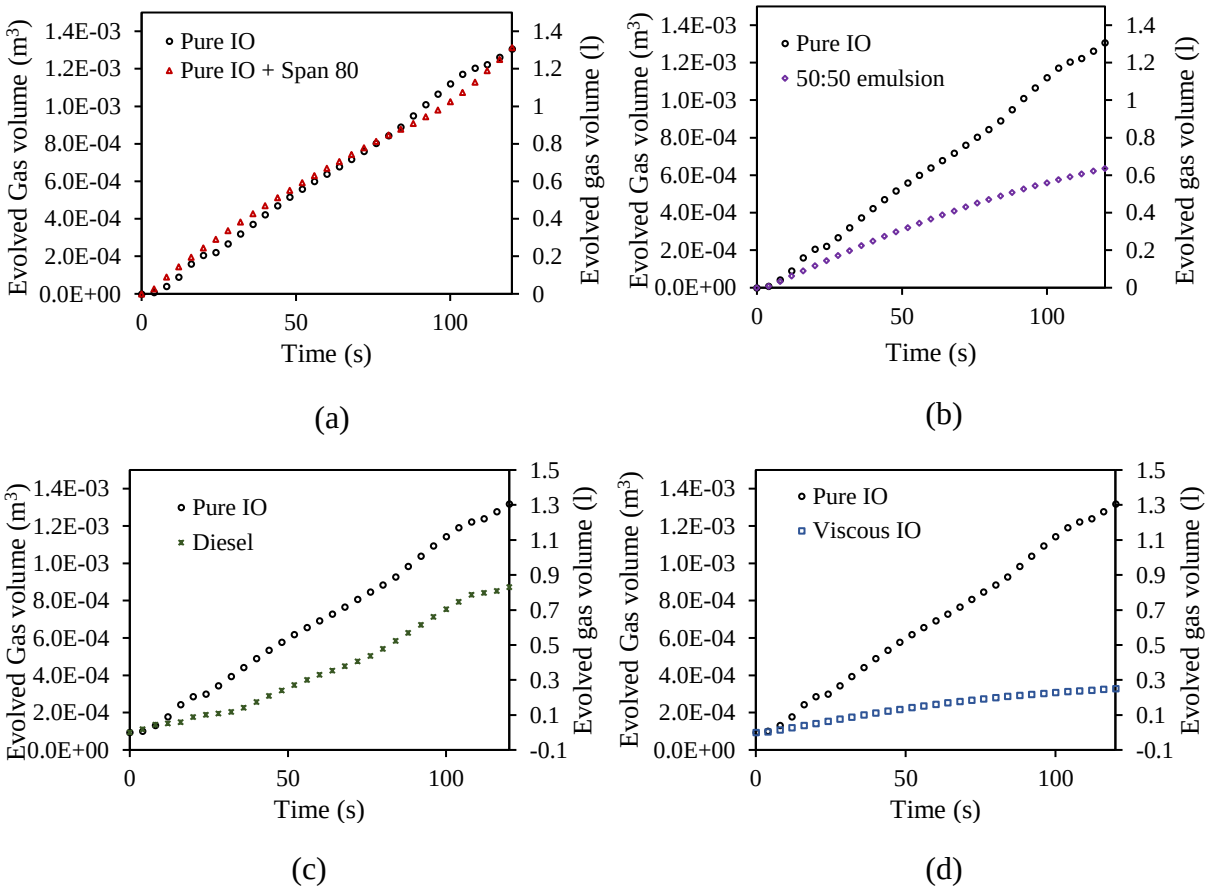

Figure 5.15. Volume of methane evolved from pure olefins compared to (a) Pure olefins + Surfactant, (b) 50:50 emulsion, (c)Diesel, (d) Viscous IO, with an initial saturation pressure of 1.38 MPa (200 psi) and depressurization rate of 0.00689 MPa/s (1 psi/s)

The rate of gas evolution from diesel was observed to be smaller than from pure olefins but was faster than 50:50 water in oil emulsions as shown in Figures 5.15b &5.15c. Gas evolution from the viscous fluid was the slowest due to increased yield point because of suspentone present in the fluid as presented in Figure 5.15d.

The degassing curve of methane from different liquid phases are shown in Figure 5.16. The concentration of methane in the liquid phases reduces over time due to the desorption of gas.

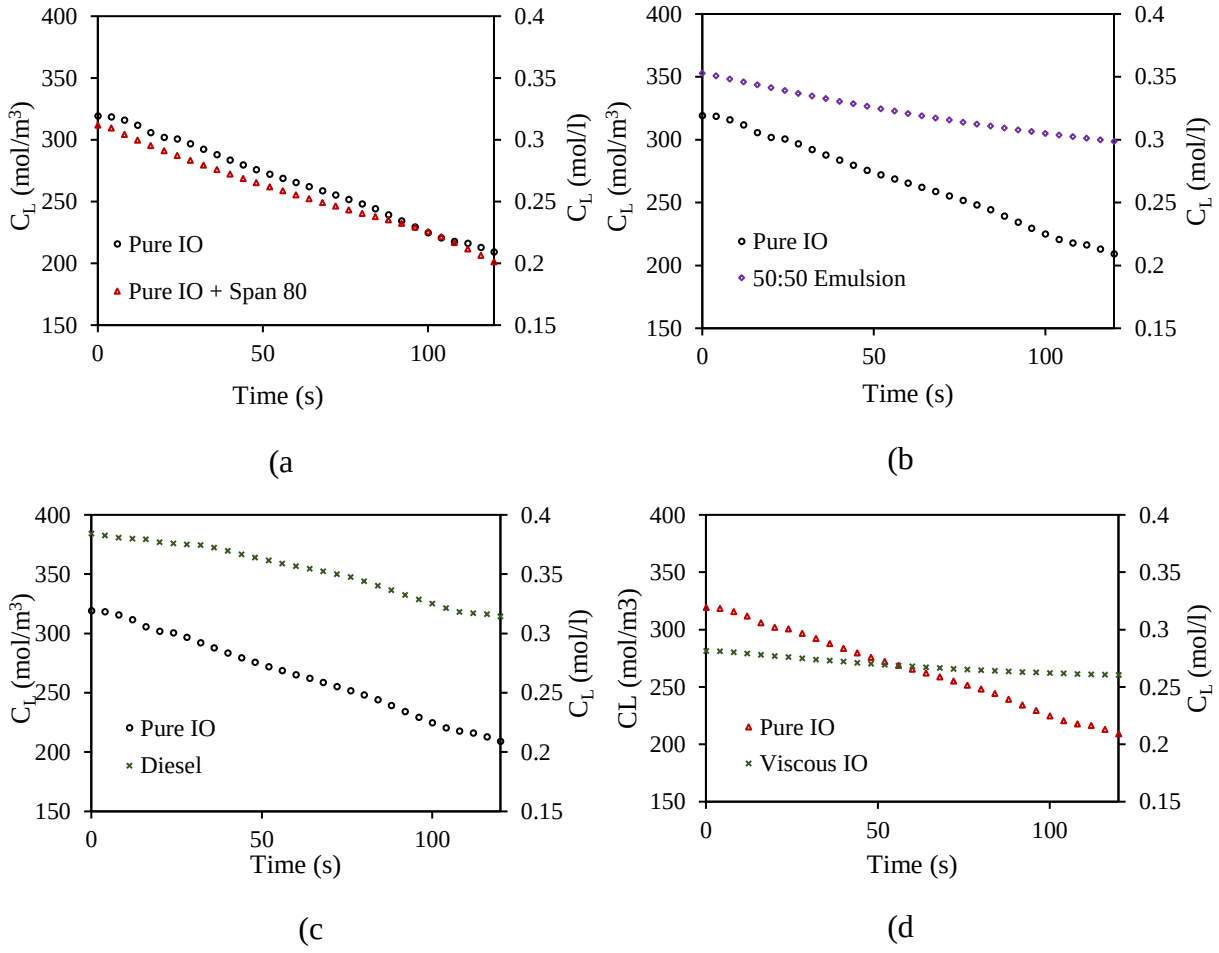

Figure 5.16. Concentration of methane during desorption from pure Olefin compared to (a) Pure IO + Surfactant, (b) 50:50 emulsion, (c)Diesel, (d) Viscous IO, with an initial saturation pressure of 1.38 MPa (200 psi) and depressurization rate of 0.00689 MPa/s (1 psi/s)

Again, degassing curves of pure olefins and olefins mixed with span 80 are similar as shown in Figure 5.16a. As illustrated in Figure 5.16b, 50:50 water-in-oil emulsion had a lower initial methane concentration and methane desorbed from it at a slower rate when compared to pure olefins. Diesel had a highest initial concentration than pure olefins as observed in Figure 5.16c, but the degassing of methane from it was slower compared to pure IO. Methane had a slower degassing rate than viscous IO as well when compared to pure IO.

Figure 5.17 shows the volumetric mass transfer coefficients for the investigated fluid systems. These coefficients are averaged values from at least two independent trials. From the figure, it is shown that at the investigated surfactant concentration, the presence of surfactant in the oil phase does not affect the mass transfer of methane from pure olefins. The addition of surfactant to pure internal olefin did not significantly affect the surface tension of the liquid phase as shown in Table 4.3, and this could be the reason for the insignificant difference in the mass transfer coefficients Miranda et al (2019) investigated the effect of surfactant using 0.1 wt. % of span 80 in Tech 80. The concentration of surfactant was extended to 2 wt. % in this study, and a similar conclusion made by Miranda et al was reached. Diesel showed a decrease in the volumetric mass transfer coefficients as compared to Olefin. This decrease was attributed to the formation of foam at the top of the liquid layer as opposed to all the evolved gas volume recorded by the flowmeter as they desorb from the liquid phase. The volumetric mass transfer coefficient of water-in-oil emulsions was lower compared to pure Olefin, which was in agreement with the observations made by Miranda et al (2019)(Miranda, Subramani, Mohammad, et al., 2020).

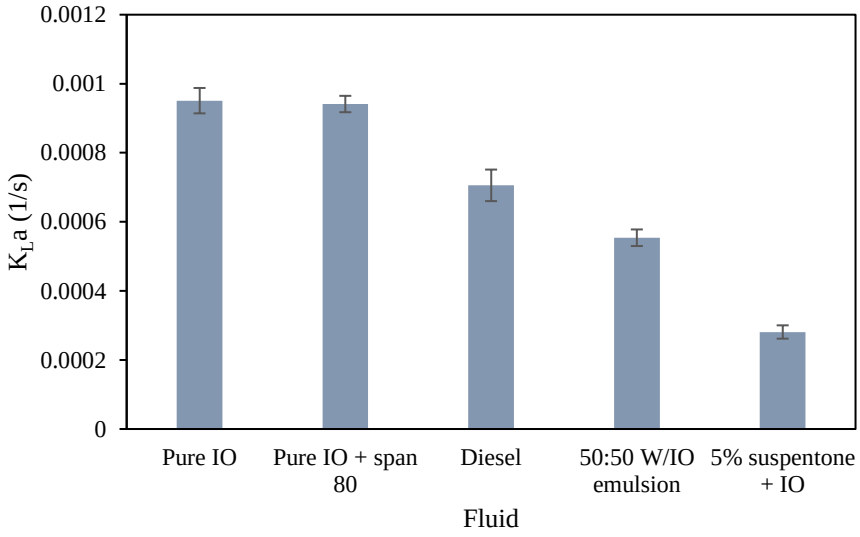

Figure 5.17: Effect of different liquid phases on the volumetric mass transfer coefficient at a depressurization rate of 0.0069MPa (1psi/s)

We hypothesized that this decrease was due to the presence of water droplets obstructing the free flow of gas out of the solution.

The desorption coefficient of methane from viscous IO (5 wt % suspentone mixed with IO) was the least among the fluid systems considered in this study. This decrease in the mass transfer coefficient was a result of the increased yield point of the liquid phase.

5.3.4. Effect of oil-water ratio of emulsion on gas evolution

A separate parametric study was carried out to understand the effect of the oil-water ratio of emulsion on gas evolution. Three different oil-water ratios, 100:0, 70:30 and 50:50, were prepared and tested with the same initial saturation pressure and depressurization rate in this study. Figure 5.18 shows that an increase in the percentage of oil content in the emulsion increases the amount of methane that dissolves in the liquid phase. This is due to oil having a significantly higher capacity to dissolve methane than water.

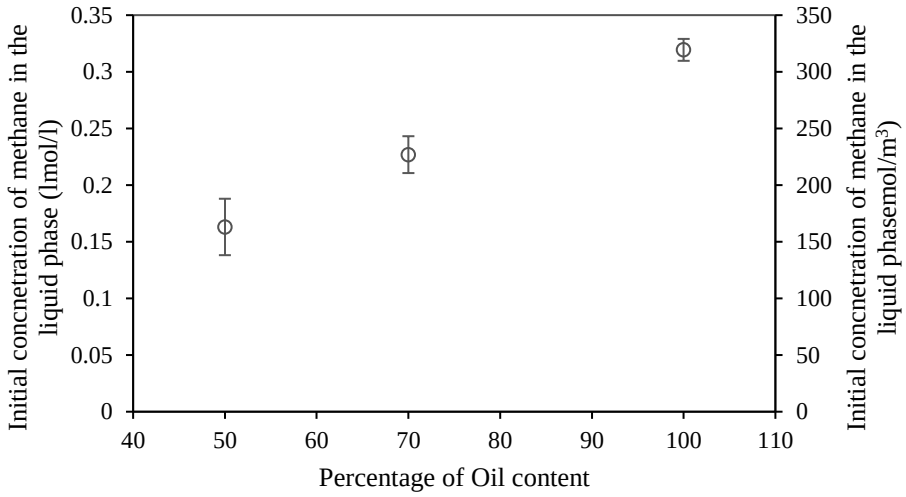

Figure 5.18. Dissolved methane concentration for emulsions with varying oil-water ratio at a depressurization rate of 0.0069MPa (1psi/s)

The cumulative evolved gas volumes for different oil-water ratios of emulsion are presented in Figure 5.19. Increase the oil content increases both the rate of gas evolution and the totalized volume of gas that evolves from solution. Figure 5.20 represents the concentration of methane in the liquid phase for different emulsion oil-water ratios. As shown in Figure 5.20, it is seen that the concentration of methane in the liquid phase across all oil-water ratios reduces with time, which indicates the desorption of gas over time. The reduction in concentration for different oil-water ratios each followed constant rate owing to the constant depressurization applied during the desorption experiments. From the Figure, it is observed that increase in the oil content led to a faster degassing rate, with pure internal olefin being the fastest to approach the new equilibrium, and 50:50 emulsion the least. Water droplets in emulsion act as an impediment to the flow of gas out of solution; therefore, as the water content reduces, there is less resistance to the flow of gas.

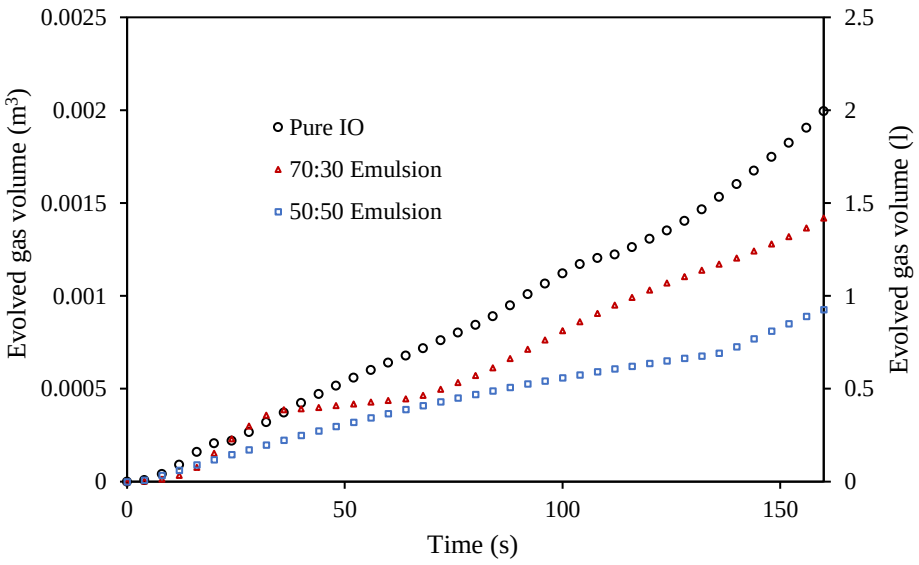

Figure 5.19. Volume of methane evolved from emulsions with different oil-water ratio at a depressurization rate of 0.0069MPa (1psi/s)

The variation of the volumetric mass transfer coefficient, with oil-water ratio is shown in Figure 5.21. For oil-water ratios considered in this study, K_La increases as the oil content in the emulsion increases.

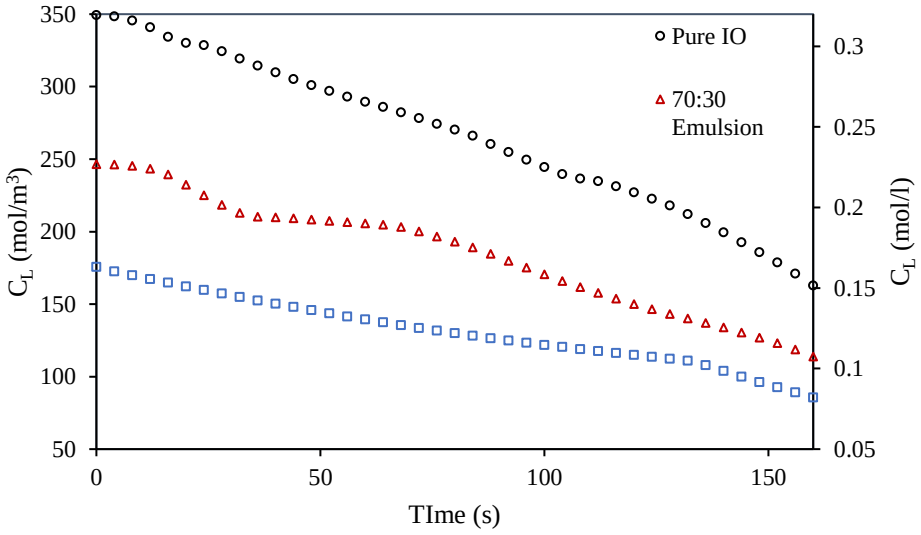

Figure 5.20. Concentration of methane in emulsions with different oil-water ratio during desorption at a depressurization rate of 0.0069MPa (1psi/s)

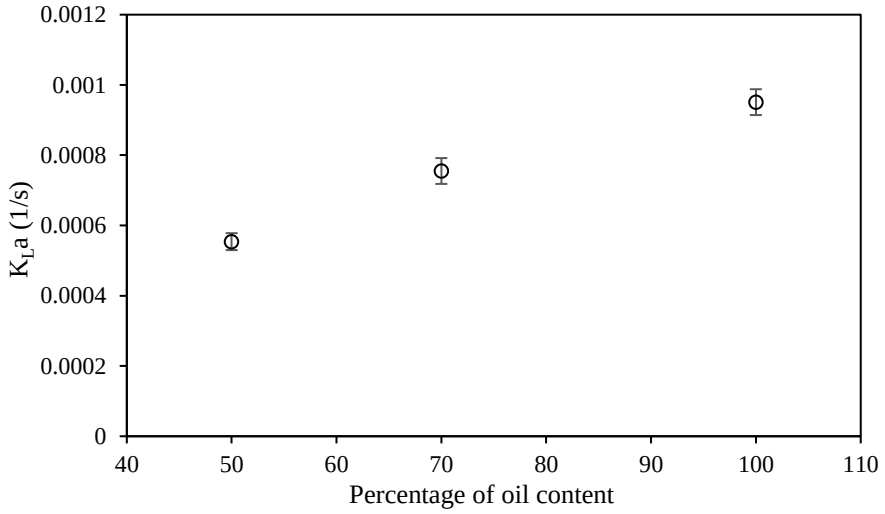

Figure 5.21. Effect of oil-water ratio of emulsion on the volumetric mass transfer coefficient at a depressurization rate of 0.0069MPa (1psi/s)

CHAPTER 6. CONCLUSION

The evolution of methane from different liquid phases was investigated in this study to tackle issues relating to the safe handling of kicks when formation gas dissolves in non-aqueous drilling fluids. A major gap in developing an advance tool that can simulate the transient multiphase flow of influxes in non-aqueous drilling fluid is the inadequate understanding of gas evolution from these fluids. One of the primary objectives of this study was therefore to develop an experimental procedure with the custom-made mass transfer apparatus, that can simulate the desorption process that could occur in a well control scenario to gain more insights into the evolution of gas bubbles from non-aqueous fluids. The initial methodology involved the use of a peak desorbed gas flow rate. Due to the restriction caused by presetting the needle to a specific peak flow rate, this methodology was modified to the rapid depressurization procedure. However, it was soon determined that the rapid depressurization experiments resulted in choked flow and does not adequately simulate the desorption process expected in a well/riser column. Eventually, the gradual depressurization experiment was adopted to remedy the issues that came with previous experimental procedures.

Using the gradual depressurization procedure, the saturated liquid phase was depressurized at constant rates to obtain data that describe gas evolution phenomenon from the liquid phases. Using methane as the gas phase with different liquid phases, gas evolution was studied for different conditions. The initial saturation pressure was varied from 0.69 to 2.07 MPa (100 to 300 psi), depressurization rates studied ranged from low rates, such as 0.0017MPa/s (0.25 psi/s), to rapid depressurization, with rate of 0.6895 MPa/s (100 psi/s). 2 vol.% of surfactants by volume of olefins and suspentone concentration of 5 wt.% of suspentone by volume of olefins were used to investigate the effects of surfactant and viscosity on gas evolution respectively. Oil-water ratio

was varied from 100:0 to 50:50 to expound the influence of oil-water ratio on mass transfer. A different liquid phase, diesel was also used as the liquid phase, and its effect on gas evolution compared to olefins was discussed.

By comparing three different initial saturation pressures (0.69, 1.38 and 2.07MPa (100, 200 and 300 psi) with two depressurization rates 0.0034 and 0.0103 MPa/s (0.5 and 1.5psi/s), it was observed that the volumetric mass transfer coefficient decreased with increasing initial saturation pressure. This decrease could be attributed to a decrease in the bubble size (and interfacial area) through which gas was coming out of solution. By varying depressurization rates, it was shown that the mass transfer coefficient increased with depressurization rate. It was postulated that this increase was because of the increased bubble frequency out of solution as depressurization rate increased. Also, the profile of gas evolution across different depressurization rates showed an increase in gas evolution rate for higher depressurization rates. A higher depressurization rate resulted in a higher driving force, which led to a higher volume of gas evolved.

The presence of surfactant was found to have an insignificant effect on gas evolution at the investigated surfactant concentration. Methane solubility in diesel was higher than in pure olefins, but the volumetric mass transfer coefficient of methane from diesel was shown to be lower compared to methane from internal olefin. Also, the mass transfer coefficient of water-in-oil emulsions were lower in comparison with pure olefins. The presence of water droplets in the continuous oil phase was attributed to this decrease. Comparing mass transfer coefficient between pure olefins and viscous olefins showed that the presence of viscosifying agents in the liquid phase decreased the volumetric mass transfer coefficient due to increased yield point. A separate sensitivity analysis was conducted for different oil water ratios. Both methane solubility in the

liquid phase and the volumetric mass transfer coefficient increased as the oil-water ratio of emulsion increased.

The results obtained from these gas evolution experiments improved the current understanding of mass transfer of a gas from non-aqueous fluids. This study again proved that desorption is indeed time dependent and not instantaneous. The mass transfer coefficients obtained from this study is valuable in incorporating the desorption kinetics in models for accurate simulation of well control events.

CHAPTER 7. RECOMMENDATIONS

The gas evolution experiments were performed using base fluids of non-aqueous drilling muds. In some cases, additives such as emulsifier and viscosifier have been added for further investigation. However, these fluid systems are not the exact representative of drilling muds used during drilling. The gas evolution experiments should be extended to actual drilling muds to understand the behavior of desorbed gas from real non-aqueous drilling fluids.

The volumetric mass transfer coefficient was found to decrease as the initial saturation pressure increased within the pressure investigated and the scale of the apparatus used in this study. However, it is yet to be confirmed if the trend will continue to hold true for pressures beyond the range tested in this study. Tests should be conducted on the larger scale system with higher pressures to confirm if the trend still holds.

Although several parameters have been investigated in this study, other parameters that could affect gas evolution outside of these parameters still exists. For instance, temperature could be a significant parameter that affects the mass transfer of methane from non-aqueous fluids. Therefore, the impact of temperature on gas evolution should be explored.

Finally, the coefficients obtained in this study were found using the small-scale experimental apparatus. Applicability of these data to a real drilling scenario, with a larger scale has not been verified. The impact of scale on the gas evolution experiments should be investigated. A mass transfer expression that is independent of the scale of the system should be identified or developed as well.

APPENDIX A. CONSIDERATION OF BLANKET GAS IN THE DERIVATION OF THE ACTUAL VOLUME OF DESORBED GAS FROM THE LIQUID PHASE.

To prevent a sudden pressure drop in the system, a blanket gas with pressure up to that in the test section I was left in the second test section to ensure a gradual pressure decrease based on the opening of the needle valve that controls the volume of gas to the flow meter.

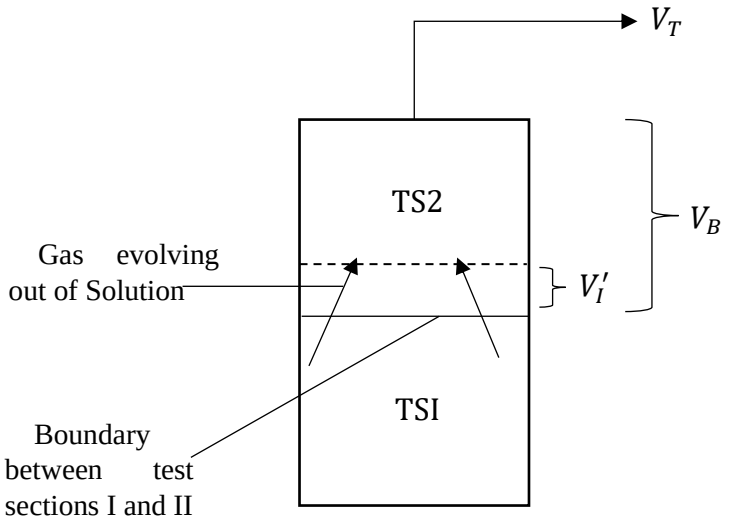

Figure A.1. Schematic of the test sections showing the dissolution of methane from diesel.

Equation A.4 and A.5 were used to obtain the actual desorbed gas volume as the experiment proceeds. This equation accounts for the presence of the blanket gas. As shown in Figure A.1, gas bubbles evolving from solution migrate through test section 2 (containing the blanket gas), to the flow meter. However, the first few volumes of gas that come out of the entire system given as V_T, comes from the blanket gas. The two equations (A.4 and A.5) provide the actual volume of gas that comes out of solution, V_1 as illustrated in the figure above.

$$V_{II} = V_T \quad \text{A.1}$$

The total volume of gas in test section II at a given time and pressure condition is equal to the total volume of voids in the test section:

$$V_I' + (V_B' - V_{II}') = V_v \quad \text{A.2}$$

V_I' is given by ideal gas law

$$V_I' = \frac{14.7 V_1 T_1}{P_1 T_0} \quad \text{A.3}$$

Put A.1, A.3, and A.4 in A.2

$$V_1 = \frac{V_v - (V_B - V_{II})\frac{14.7 T_1}{P_1 T_0}}{\frac{14.7 T_1}{P_1 T_0}} \quad \text{A.4}$$

When $V_T > V_B$

$$V_I = V_T - V_B + \frac{V_v P T_0}{14.7 T_1} \quad \text{A.5}$$

$P = P_1$ When $V_T = V_B$

APPENDIX B. TEST MATRICES FOLLOWED DURING THE EXPERIMENTAL DEVELOPMENT

Table B.1. Tests followed for the peak flow rate experiments

S/N	Trials	Base Fluid Type	Pressure (psig)	Peak discharge flow rate (ln/min)
1	2	Diesel	100	5
2				10
3				15
4				20
5				25
6			125	5
7				10
8				15
9				20
10				25
11			150	5
12				10
13				15
14				20
15				25
16			200	5
17				10
18				15
19				20
20				25

Table B.2. Test matrix followed for the rapid depressurization experiments

S/N	Trials	Base Fluid Type	Pressure (psig)	Concentration of Suspentone (wt.%) by volume of liquid)
1	2	Olefins	150	0
2				2.5
3				5

APPENDIX C. CORRECTION OF THE LATENCY OF FLOW RATE MEASUREMENT

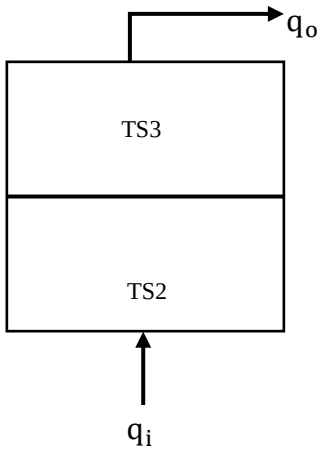

Figure C.1. Schematic of the test sections.

To compensate for the lag between the time gas evolves from solution in the first test section and the time it takes the flow meter to detect the flow of gas, a mass balance is done around the second and third test section.

$$\text{mass in} - \text{mass out} = \text{change in accumulation} \tag{C.1}$$

$$\rho(q_i - q_o)\Delta t = \Delta m \tag{C.2}$$

From gas law,

$$\rho = \frac{PM}{RT} \tag{C.3}$$

and

$$\Delta m = \frac{P_t VM}{RT} - \frac{P_{t=0} VM}{RT} \quad \text{C.4}$$

$$\Delta m = \frac{VM}{RT}(P_t - P_{t=0}) \quad \text{C.5}$$

Put Eqn. C3 and C5 in C2

$$\frac{PM}{RT}(q_i - q_o)\Delta t = \frac{VM}{RT}(P_t - P_{t=0}) \quad \text{C.6}$$

$$q_i - q_o = \frac{V}{P\Delta t}(P_t - P_{t=0}) \quad \text{C.7}$$

$$q_i = q_o + \frac{V}{P\Delta t}(P_t - P_{t=0}) \quad \text{C.8}$$

BIBLIOGRAPHY

Al-Hindi, M., & Azizi, F. (2018). Absorption and desorption of carbon dioxide in several water types. *The Canadian Journal of Chemical Engineering, 96*(1), 274-284.

Avelar, C. S., Ribeiro, P. R., & Sepehrnoori, K. (2009). Deepwater gas kick simulation. *Journal of Petroleum Science and Engineering, 67*(1-2), 13-22.

Barrut, B., Blancheton, J.-P., Champagne, J.-Y., & Grasmick, A. (2012). Mass transfer efficiency of a vacuum airlift—Application to water recycling in aquaculture systems. *Aquacultural engineering, 46*, 18-26.

Becerra, E., & Parise, J. (2003). *Experimental study of foam formation during refrigerant desorption from a R134a/polyolester lubricating oil mixture.* Paper presented at the Proc. Int. Congress Refrig.

Bjørkevoll, K. S., Skogestad, J. O., Frøyen, J., & Linga, H. (2018). *Well Control Simulator: Enhancing Models with Compositional PVT Models and Kinetics.* Paper presented at the IADC/SPE Drilling Conference and Exhibition.

Blázquez, C., Dalmazzone, C., Emond, E., & Schneider, S. (2016). Crude oil foams. Part 1–A novel methodology for studying non-aqueous foams formed by depressurization. *Fuel, 171*, 224-237.

Boesch, D. F., & Rabalais, N. N. (1987). *Long-term environmental effects of offshore oil and gas development*: CRC Press.

Boyd, C. E. (1986). A method for testing aerators for fish tanks. *The Progressive Fish-Culturist, 48*(1), 68-70.

Caenn, R., Darley, H. C., & Gray, G. R. (2011). *Composition and properties of drilling and completion fluids*: Gulf professional publishing.

Colt, J., Watten, B., & Pfeiffer, T. (2012). Carbon dioxide stripping in aquaculture–Part II: Development of gas transfer models. *Aquacultural engineering, 47*, 38-46.

Daniel, A. B. (2018). *Gas Evolution and Gas-Liquid Separator Modeling.*

Daniel, A. B., Mohammad, S. A., Miranda, M. A., & Aichele, C. P. (2019). Absorption and desorption mass transfer rates as a function of pressure and mixing in a simple hydrocarbon system. *Chemical Engineering Research and Design, 144*, 209-215.

de Carvalho, M. A. D., de Moraes Oliveira, G. F., Fernandes, L. D., Martins, A. L., Vega, M. P. J. J. o. P. S., & Engineering. (2019). Two-phase flow model validation during conventional/Pressurized Mud Cap Drilling (PMCD) scenarios. *172*, 314-326.

Eshchar, M., Mozes, N., & Fediuk, M. (2003). Carbon dioxide removal rate by aeration devices in marine fish tanks.

Evje, S., & Fjelde, K. K. (2002). Hybrid flux-splitting schemes for a two-phase flow model. *Journal of Computational Physics, 175*(2), 674-701.

Fortkamp, F. P., & Barbosa Jr, J. R. (2015). Refrigerant desorption and foaming in mixtures of HFC-134a and HFO-1234yf and a polyol ester lubricating oil. *International Journal of Refrigeration, 53*, 69-79.

Fraser, D., Lindley, R., Moore, D. D., & Vander Staak, M. (2014). *Early kick detection methods and technologies.* Paper presented at the SPE Annual Technical Conference and Exhibition.

Gevantman, L. (2000). Solubility of selected gases in water. *Nitric oxide (NO), 308*(3.348), 10-14.

Gomes, D., Nilsen, M. S., Frøyen, J., Bjørkevoll, K. S., Lage, A. C., Fjelde, K. K., & Sui, D. (2018). *A Transient Flow Model for Investigating Parameters Affecting Kick Behavior in OBM for HPHT Wells and Backpressure MPD Systems.* Paper presented at the ASME 2018 37th International Conference on Ocean, Offshore and Arctic Engineering.

Goswami, D., Shah, D., Jotshi, C., Bhagwat, S., Leung, M., & Gregory, A. (1997). *Foaming characteristics of refigerant/lubricant mixtures*. Retrieved from

Grace, R. D. (2017). *Blowout and well control handbook*: Gulf Professional Publishing.

Grimstad, A.-A., Linga, H., Haave, Ø., & Saasen, A. (2017). *Degassing rate of drilling fluid base oils as exposed to depressurisation and drill string rotation.* Paper presented at the SPE/IADC Drilling Conference and Exhibition.

Growcock, F. B., & Patel, A. D. (2011). *The revolution in non-aqueous drilling fluids.* Paper presented at the Proceedings at the 2011 AADE National Technical Conference and Exhibition.

Gu, Q., Fallah, A., Feng, T., Bakshi, S., Chen, D., Ashok, P., . . . van Oort, E. (2021). A novel dilution control strategy for gas kick handling and riser gas unloading mitigation in deepwater drilling. *Journal of Petroleum Science and Engineering, 196*, 107973.

Hamborg, E. S., Kersten, S. R., & Versteeg, G. F. J. C. E. J. (2010). Absorption and desorption mass transfer rates in non-reactive systems. *161*(1-2), 191-195.

Hemmingsen, E. A. (1975). Cavitation in gas− supersaturated solutions. *Journal of Applied Physics, 46*(1), 213-218.

Hikita, H., & Konishi, Y. (1984). Desorption of carbon dioxide from supersaturated water in an agitated vessel. *AIChE journal, 30*(6), 945-951.

Huerta, M., Otero, C., Rico, A., Jimenez, I., de Mirabal, M., & Rojas, G. (1996). *Understanding foamy oil mechanisms for heavy oil reservoirs during primary production.* Paper presented at the SPE Annual Technical Conference and Exhibition.

Jeelani, S., Fidi, N., & Hartland, S. (1990). Foam formation during CO2 desorption from agitated supersaturated aqueous surfactant solutions. *Chemical engineering science, 45*(4), 1043-1048.

Jones, S., Evans, G., & Galvin, K. (1999). Bubble nucleation from gas cavities—a review. *Advances in colloid and interface science, 80*(1), 27-50.

Kierzkowska-Pawlak, H., & Chacuk, A. (2010). Carbon dioxide desorption from saturated organic solvents. *Chemical Engineering & Technology: Industrial Chemistry-Plant Equipment-Process Engineering-Biotechnology, 33*(1), 74-81.

Kim, Y., Han, K., & Lee, W. (2003). Removal of organics and calcium hardness in liner paper wastewater using UASB and CO2 stripping system. *Process Biochemistry, 38*(6), 925-931.

Kim, Y. H., Yeom, S. H., Ryu, J. Y., & Song, B. K. (2004). Development of a novel UASB/CO2-stripper system for the removal of calcium ion in paper wastewater. *Process Biochemistry, 39*(11), 1393-1399.

King, M. B. (2013). *Phase Equilibrium in Mixtures: International Series of Monographs in Chemical Engineering* (Vol. 9): Elsevier.

Lavenson, D. M., Kelkar, A. V., Daniel, A. B., Mohammad, S. A., Kouba, G., & Aichele, C. P. (2016). Gas evolution rates–A critical uncertainty in challenged gas-liquid separations. *Journal of Petroleum Science and Engineering, 147*, 816-828.

Lekvam, K., & Bishnoi, P. R. (1997). Dissolution of methane in water at low temperatures and intermediate pressures. *Fluid Phase Equilibria, 131*(1-2), 297-309.

Lewis, W., & Whitman, W. (1924). Absorption symposium. *Ind. Eng. Chem., 16*(12), 1215-1220.

Lisitsin, D., Hasson, D., & Semiat, R. (2008). The potential of CO2 stripping for pretreating brackish and wastewater desalination feeds. *Desalination, 222*(1-3), 50-58.

Ma, Z., Vajargah, A. K., Ambrus, A., Ashok, P., Chen, D., Van Oort, E., . . . Becker, G. (2017). *A comprehensive hydraulic software package for drilling operations.* Paper presented at the AADE National Technical Conference and Exhibition, Houston, Texas, USA.

Ma, Z., Vajargah, A. K., Ambrus, A., Ashok, P., Chen, D., van Oort, E., . . . Curry, D. A. (2016). *Multi-Phase Well Control Analysis During Managed Pressure Drilling Operations*. Paper presented at the SPE Annual Technical Conference and Exhibition, Dubai, UAE. https://doi.org/10.2118/181672-MS

Ma, Z., Vajargah, A. K., Chen, D., van Oort, E., May, R., MacPherson, J., . . . Curry, D. (2018). *Gas kicks in non-aqueous drilling fluids: a well control challenge.* Paper presented at the IADC/SPE Drilling Conference and Exhibition.

Manikonda, K. (2020). *Modeling Gas Kick Behavior in Water and Oil-Based Drilling Fluids.*

Miranda, M. A., Subramani, H. J., & Aichele, C. P. (2020). Impact of Supersaturation Ratio on the Kinetics of Gas Evolution at Elevated Pressures. *Energy & Fuels, 34*(12), 15812-15818.

Miranda, M. A., Subramani, H. J., Mohammad, S. A., & Aichele, C. P. (2020). Kinetics of Gas Evolution from Supersaturated Oils at Elevated Pressures and Temperatures. *Energy & Fuels*.

Miranda, M. A., Yegya Raman, A. K., Lavenson, D. M., Subramani, H. J., Mohammad, S. A., & Aichele, C. P. (2019). Gas Evolution Rates in Supersaturated Water-in-Oil Emulsions at Elevated Pressures. *Energy & Fuels, 33*(9), 8176-8183.

Nickens, H. (1987). A dynamic computer model of a kicking well. *SPE Drilling engineering, 2*(02), 159-173.

Nwaka, N., & Chen, Y. (2019). *Numerical simulations of riser gas behavior in non-aqueous muds using a modified drift flux model.* Paper presented at the ASME 2019 38th International Conference on Ocean, Offshore and Arctic Engineering.

Nwaka, N., Wei, C., Ambrus, A., & Chen, Y. (2020). Gas in riser: On modeling gas influxes in non-aqueous drilling fluids with time-dependent desorption considerations. *Journal of Petroleum Science and Engineering, 195*, 107785.

O'Bryan, P. L. (1985). *The experimental and theoretical study of methane solubility in an oil-base drilling fluid.* Louisiana State University, Baton Rouge,

Ojedeji, D., & Chen, Y. (2020). *Effect of the Concentration of Viscosifier on Desorption Kinetics of Methane From Synthetic Based Fluids.* Paper presented at the International Conference on Offshore Mechanics and Arctic Engineering.

Ojedeji, D., Perry, S., Nielsen, J., & Chen, Y. (2020). Experimental investigation of desorption kinetics of methane in diesel and internal olefin for enhanced well control. *Greenhouse Gases: Science and Technology, 10*(2), 364-379.

Panja, N., & Phaneswararao, D. (1994). Volumetric Mass-Transfer Coefficients from Desorption Data. *Chemical engineering research & design, 72*(5), 633-638.

Podio, A., & Yang, A.-P. (1986). *Well control simulator for IBM personal computer.* Paper presented at the IADC/SPE Drilling Conference.

Pooladi-Darvish, M., & Firoozabadi, A. (1999). Solution-gas drive in heavy oil reservoirs. *Journal of Canadian Petroleum Technology, 38*(04).

Rixon, F. (1948). The absorption of carbon dioxide in and desorption from water using packed towers. *Trans. Inst. Chem. Eng, 26*, 119.

Sheng, J., Maini, B., Hayes, R., & Tortike, W. (1999). A non-equilibrium model to calculate foamy oil properties. *Journal of Canadian Petroleum Technology, 38*(04).

Sherwood, T., Draemel, F., & Ruckman, N. (1937). Desorption of carbon dioxide from water in a packed tower. *Industrial & Engineering Chemistry, 29*(3), 282-285.

Sherwood, T., & Holloway, F. (1940). Performance of packed towers-liquid film data for several packings. *Transactions of the American Institute of Chemical Engineers, 36*(1), 39.

Shulman, H. L., & Molstad, M. (1950). Gas-bubble columns for gas-liquid contacting. *Industrial & Engineering Chemistry, 42*(6), 1058-1070.

Simoneau, R. J. (1981). Depressurization and two-phase flow of water containing high levels of dissolved nitrogen gas. *NASA STI/Recon Technical Report N, 81*, 28389.

Skogestad, J. O., Bjørkevoll, K. S., Frøyen, J., Linga, H., Lenning, E., & Håvardstein, S. T. (2019). *Well Control Incident in the North Sea as Interpreted with Advanced Gas Influx Modelling.* Paper presented at the SPE/IADC International Drilling Conference and Exhibition.

Swanson, B., Gilvary, B., & McEwan, F. (1988). *Experimental measurement and modeling of gas solubility in invert emulsion drilling fluids explains surface observations during kicks.* Paper presented at the European Petroleum Conference.

Szebehely, V. (1951). Relation between gas evolution and physical properties of liquids. *Journal of Applied Physics, 22*(5), 627-628.

Thuy, L., & Weiland, R. (1976). Mechanisms of gas desorption from aqueous solution. *Industrial & Engineering Chemistry Fundamentals, 15*(4), 286-293.

Torsvik, A., Skogestad, J., & Linga, H. J. H.-T. W. S. o. P. E. d. (2017). An Experimental Study of Gas Influx in Oil-Based Drilling Fluids for Improved Modeling of High-Pressure. *10*.

Tunnat, A., Behr, P., & Görner, K. (2014). Desorption kinetics of CO2 from water and aqueous amine solutions. *Energy Procedia, 51*, 197-206.

Voyer, R., & Miller, A. (1968). Improved gas' liquid contacting in co-current flow. *The Canadian Journal of Chemical Engineering, 46*(5), 335-341.

Wang, C., Xu, R., Chen, X., Jiang, P., & Liu, B. (2019). Study on water flash evaporation under reduced pressure. *International Journal of Heat and Mass Transfer, 131*, 31-40.

Weiland, R. H., Thuy, L. T., & Liveris, A. N. (1977). Transition from bubbling to quiescent desorption of dissolved gases. *Industrial & Engineering Chemistry Fundamentals, 16*(3), 332-335.

Weiss, R. F. (1974). Carbon dioxide in water and seawater: the solubility of a non-ideal gas. *Marine chemistry, 2*(3), 203-215.

Xu, Z., Song, X., Li, G., Zhu, Z., & Zhu, B. (2019). Gas kick simulation in oil-based drilling fluids with the gas solubility effect during high-temperature and high-pressure well drilling. *Applied Thermal Engineering, 149*, 1080-1097.

VITA

Damilola O. Ojedeji received his bachelor's degree in petroleum engineering from the University of Lagos, Nigeria. He previously had his internship at Total exploration and production Nigeria limited as a production performance intern. Then he worked for a year at the center for research and development, Federal University of technology, Akure, Nigeria. He began his education at the Louisiana State University in 2019 to earn his master's degree in petroleum engineering. He anticipates graduating in the summer of 2021 with his master's in petroleum engineering. He has accepted an offer from the University of Tennessee, Knoxville to begin his PhD in Chemical Engineering in the Fall of 2021.